REPORT DOCUMENTATION PAGE

FORM APPROVED
OMB No. 0704-0188

1. AGENCY USE ONLY (Leave blank)	2. REPORT DATE	3. REPORT TYPE AND DATES COVERED
		Quarter - March 1, 1996 through May 31, 1996

4. TITLE AND SUBTITLE OF REPORT
Visible Light Emitting Materials and Injection Devices

5. FUNDING NUMBERS
ONR Grant
N00014-92-J-1895

6. AUTHOR(S)
Paul H. Holloway

7. PERFORMING ORGANIZATION NAME(S) AND ADDRESS(ES)
Department of Materials Science and Engineering
University of Florida
P.O. Box 116400
Gainesville, FL 32611-6400

8. PERFORMING ORGANIZATION REPORT NUMBER:
N/A

9. SPONSORING/MONITORING AGENCY NAME(S) AND ADDRESS(ES)
Office of Naval Research
800 North Quincy Street
Arlington, VA 22217-5000

10. SPONSORING/MONITORING AGENCY REPORT NUMBER:

11. SUPPLEMENTARY NOTES:

12a. DISTRIBUTION AVAILABILITY STATEMENT
Unlimited

12b. DISTRIBUTION CODE

13. ABSTRACT (Maximum 200 words)

Progress in report on research into ZnSe-based and GaN-based materials and devices for light emitting diodes and diode lasers at blue-green visible wavelengths.

14. SUBJECT TERMS	15. NUMBER OF PAGES: 65
	16. PRICE CODE

17. SECURITY CLASSIFICATION OF REPORT: None	18. SECURITY CLASSIFICATION OF THIS PAGE None	19. SECURITY CLASSIFICATION OF ABSTRACT None	20. LIMITATION OF ABSTRACT None

DISCLAIMER NOTICE

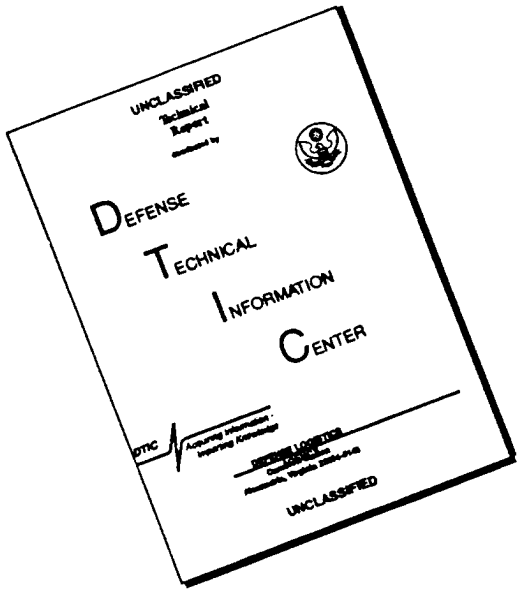

THIS DOCUMENT IS BEST QUALITY AVAILABLE. THE COPY FURNISHED TO DTIC CONTAINED A SIGNIFICANT NUMBER OF PAGES WHICH DO NOT REPRODUCE LEGIBLY.

Quarterly Progress Report

March 1, 1996 to May 31, 1996

Visible Light Emitting Materials and Injection Devices

ONR/DARPA URI

Grant Number N00014-92-J-1895

Prepared by:

Paul H. Holloway
Department of Materials Science and Engineering
University of Florida
P.O. Box 116400
Gainesville, FL 32611
Ph: 352/392-6664; FAX: 352/392-4911
E-Mail: Internet - pholl@silica.mse.ufl.edu

Participants:
University of Florida
Kevin Jones
Robert Park
Joseph Simmons
Cammy Abernathy
Stephen Pearton
Dept. of Materials Science and Engineering
Timothy Anderson
Dept. of Chemical Engineering
Peter Zory
Dept. of Electrical Engineering
Columbia University
Gertrude Neumark
Dept. of Materials Science and Engineering
Oregon Graduate Institute of Science and Engineering
Reinhart Engelmann
Dept. of Electrical Engineering
University of Colorado at Boulder
Jacques Pankove
Dept. of Electrical Engineering

(I) Growth by MBE and Characterization of GaN (Robert Park)

I.a. II-VI Work

Our recent activities in the II-VI area have focused on stacking fault density reduction in ZnSe epilayers and the attached manuscript (see Appendix 1), which has been submitted to Applied Physics Letters (4/18/96), summarizes our recent results. This work is also supported in part by the II-VI Consortium.

In summary, we have determined that the surface stoichiometry maintained during the first five monolayers of ZnSe epitaxial growth can have a significant influence on the stacking fault concentration in 2μm thick epilayers. In particular, we have been able to minimize the stacking fault concentration to a level in the 10^4 cm^{-2} range (comparable to the stacking fault concentration in the ZnSe substrates used for epitaxy) by appropriate selection of a delay time (approximately 30 seconds for a substrate temperature of 300°C) employed during an alternate element (Zn and Se) exposure phase of growth. The delay time in question is the time elapsed between closing the Se shutter and opening the Zn shutter.

We have found that the surface stoichiometry (Zn to Se atomic ratio) can be tailored during the delay phase since Se thermal desorption occurs at the growth temperature in a controlled fashion from an initially Se-terminated surface, and, we postulate that selection of an optimum delay time, corresponding to the attainment of a near-stoichiometric surface, results in the growth of low stacking fault concentration material.

I.b. III-V Nitride Work

Further optimization of deposition parameters for the growth of cubic-GaN on MgO has resulted in the production of higher quality material as evidenced by the low-temperature PL spectrum shown in Fig. I.1. As can be seen from the spectrum, a relatively sharp peak is dominant at 3.28 eV (at 21.5K).

The energy of this dominant peak was determined as a function of sample temperature over the range, 21K to 300K, and the data obtained are plotted in Fig. I.2. The data has been fitted using the Varshni approximation method to the theoretical bandgap. As can be seen from the figure, the data fits well for temperatures in the 150 to 300K range. Based on this range, a fitting parameter, A, was obtained having a value of 6.3×10^{-4} $eV \bullet K^{-1}$, and a zero Kelvin bandgap of 3.297 eV was obtained for the cubic material. As can be seen from Fig. I.2, however, the experimental data points deviate from the theoretical curve at temperatures lower than about 150K and we are presently trying to understand this deviation.

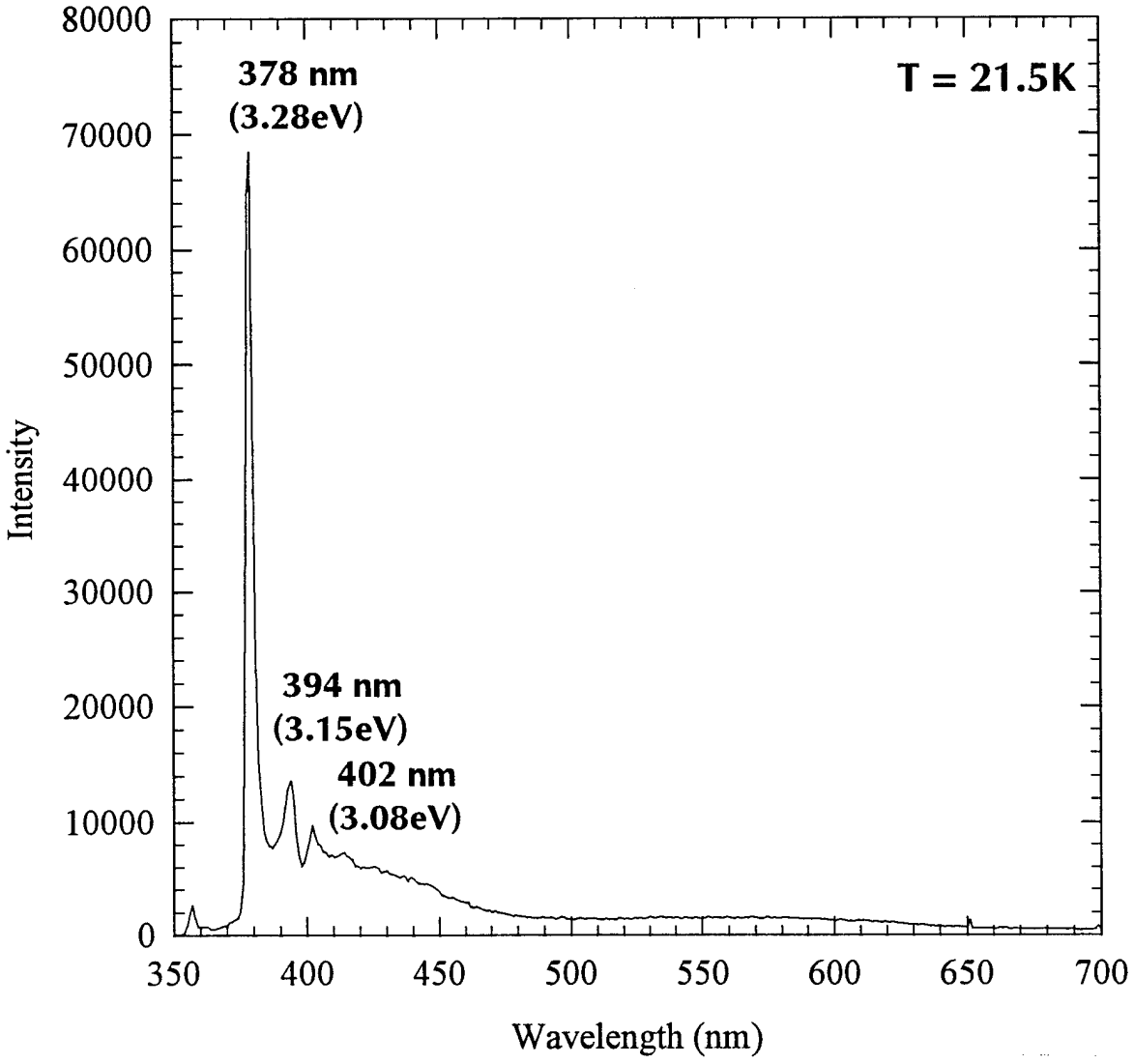

Fig. I.1. PL spectrum of β-GaN/MgO

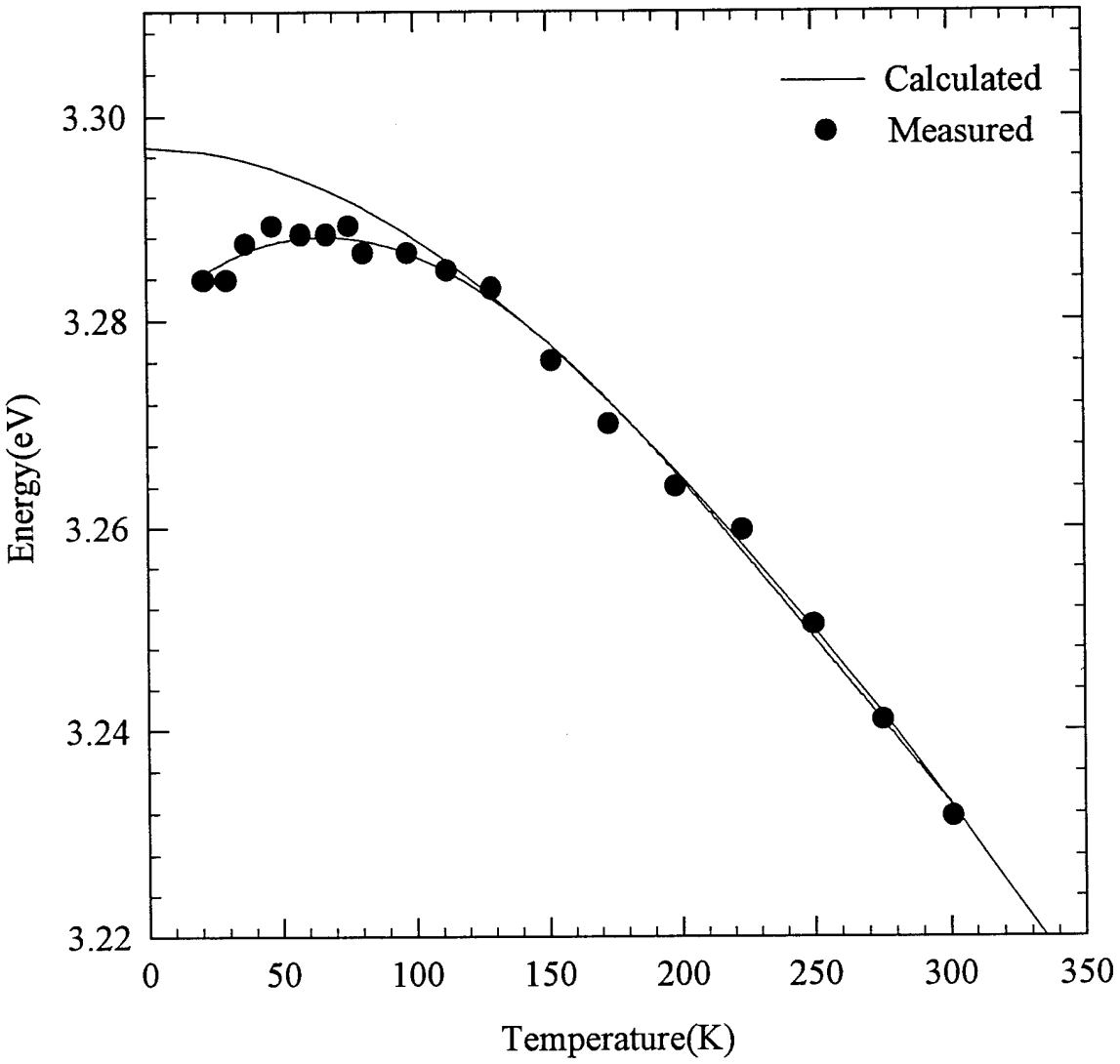

Fig. I.2. Bandgap Energy vs. Temp. for Cubic GaN/MgO

(II) Growth and processing of GaN-based materials (Cammy Abernathy and Steve Pearton)

II.a. Wet and Dry Etching of $LiGaO_2$ and $LiAlO_2$ substrates for III-nitride epitaxy

GaN and related alloys are generally grown on (0001) Al_2O_3 substrates in spite of the large lattice mismatch (~14% for GaN), due to the lack of commercially available bulk single crystal nitrides. The Al_2O_3 is relatively inexpensive, available in large diameters, stable at the nitride growth temperatures and simple to clean. Growth of AlGaN/InGaN heterostructures on Al_2O_3 has led to the high brightness light-emitting diodes and lasers reported by Nakamura et al. Alternative substrates that have been employed include SiC (3.1% lattice mismatch to GaN for the 6H polytype), which is attractive because it is cleavable and available in doped form, but is expensive and difficult to clean. They also include $MgAl_2O_4$ which has a 10% mismatch with GaN and is cleavable, ZnO, MgO, Si and III-V materials such as GaAs and InP. Thick GaN layers grown by vapor phase epitaxy on Al_2O_3 substrates have been employed as templates for GaN homoepitaxy by removing the Al_2O_3, and the first report on growth on small bulk GaN crystals recently appeared. The high dissociation pressure of nitrogen (15 kbar) at the growth temperature (1,600°C) makes bulk GaN crystals difficult to produce on a large scale.

Two promising substrates for nitride epitaxy are the wurtzite crystals $LiGaO_2$ and $LiAlO_2$, which have a-axis mismatches of +0.19% and -1.45%, respectively, to GaN. These are grown by the Czochralski technique in diameters currently up to 1.5 inches, and have bandgaps of 6.5eV ($LiAlO_2$) and 5.6eV ($LiGaO_2$). Both were (100) oriented. Dissociation of these materials at the typical Metal Organic Chemical Vapor Deposition growth temperature of ~1040°C may restrict their use to the Molecular Beam Epitaxy techniques, but promising x-ray and photoluminescence results have already been reported for AlGaN/GaN structures grown on $LiGaO_2$. Growth on patterned substrates, or creation of through-wafer via holes for microwave power electronics, requires that etching processes be developed for both materials. We report several wet etch solutions for $LiGaO_2$ and $LiAlO_2$, and compare three different dry etch chemistries in terms of rate, surface morphology and anisotropy. We have found that these materials may be wet chemically etched in a number of acid solutions, including HF, at rates between 150-40,000 Å/min. Dry etching with SF_6/Ar plasmas provides faster rates than Cl_2/Ar or CH_4/H_2/Ar under Electron Cyclotron Resonance conditions, indicating the fluoride etch products are more volatile that their chloride or metalorganic/hydride counterparts.

The polished faces of both materials were patterned either with AZ5209E photoresist or a carbon-based mask in a resolution test array with feature sizes from 0.5-200μm. Dry etching was performed in a Plasma Therm SLR 770 system utilizing an Astex 4400 Electron Cyclotron Resonance (ECR) source operating at 2.45GHz and at powers up to 1000W. The Si carrier wafer is mechanically clamped to a He backside cooled, rf powered chuck. The process pressure was varied from 1-20mTorr, but was held at 1.5mTorr for most runs. Three different plasma chemistries, Cl_2/Ar, CH_4/H_2/Ar and

SF_6/Ar, were investigated since they enable us to determine which of the typical types of etch products (i.e. chlorides, metalorganic/hydride, or fluoride, respectively) are most volatile for the oxide substrates. Etch rates were determined by stylus profilometry after removal of the mask materials and surface morphology was examined by scanning electron microscopy and atomic force microscopy.

Figure II.1 shows etch depth versus time for $LiAlO_2$ and $LiGaO_2$ in various wet etch solutions at 25°C. The etch rates were very high (~3-4μm/min) for $LiAlO_2$ with HF, and for $LiGaO_2$ with HCl and HF. More controlled rates (150-350Å/min) were obtained for $LiAlO_2$ with H_3PO_4, HNO_3 and H_2SO_4. Note that HCl is highly selective for $LiGaO_2$ over $LiAlO_2$. Most of the solutions provided linear etch depth with time, an absence of etch rate dependence on agitation, and smooth surface morphologies. These are all characteristics of reaction-limited etching where the rate-limiting step is formation and dissociation of the etch products. The exception was HF, which for both materials was found to have a square root dependence of etch depth on solution immersion time, and whose rate was a strong function of agitation. The morphology of the etched surface was also considerably rougher than those obtained with the other solutions. These are all hallmarks of diffusion-controlled etching, where the rate is controlled by diffusion of the reactant to the gallate or aluminate surface. This is a less attractive situation for reproducible etch processing because it is more difficult to achieve the same degree of agitation in a mixture than to control its temperature, which is the key parameter in reaction-limited etching. An SEM micrograph of features etched into $LiGaO_2$ with HF is shown at the top of Fig. II.2. The extensive undercut on the sidewalls is typical of wet etching. As mentioned above, the etched surface morphology for both $LiGaO_2$ and $LiAlO_2$ in HF solutions was worse (typically by a factor of approximately five in terms of root mean square roughness) than with the other etchants investigated. We did not study in detail the crystallographic dependence of the wet etching.

Fig. II.3 shows the etch rate of $LiGaO_2$ in ECR plasmas of $5CH_4/15H_2/25Ar$, $5Cl_2/10Ar$ or $5SF_6/10Ar$ (where the numbers refer to the individual gas flow rates in standard cubic centimeters per minute), as a function of rf power. The microwave power was held constant at 1000 W, and the process pressure was 1.5 mTorr. These etch conditions are typical of those we employed for etching III-V materials, including GaN ($CH_4/H_2/Ar$) or dielectrics (SF_6/Ar). We obtained similar rates for $LiAlO_2$ in all three mixtures, and show only those for SF_6/Ar. The fluoride etch products appear to be the most volatile, and for each plasma chemistry the etch rates continue to increase with rf power due to two reasons. Firstly, the increased average ion energy at higher rf powers is more efficient at initially breaking the bonds in the substrate material, which must precede etch product formation, and secondly, there is more efficient sputter-enhanced removal of the products once they form. The first mechanism has been found to be the rate-limiting step in dry etching of GaN and AlN, which have volatile chloride etch products but very stable bonding that must be overcome before the products can form. In addition, the LiF_X, GaF_X and AlF_X species that form in SF_6/Ar plasmas have quite low volatilites and must be removed by sputter assistance. An SEM micrograph of features etched into $LiGaO_2$ with a Cl_2/Ar ECR plasma (1000 W microwave power, 1.5 mTorr, 250 W rf power) is shown at the bottom of Fig. II.2. The etched surface is quite smooth

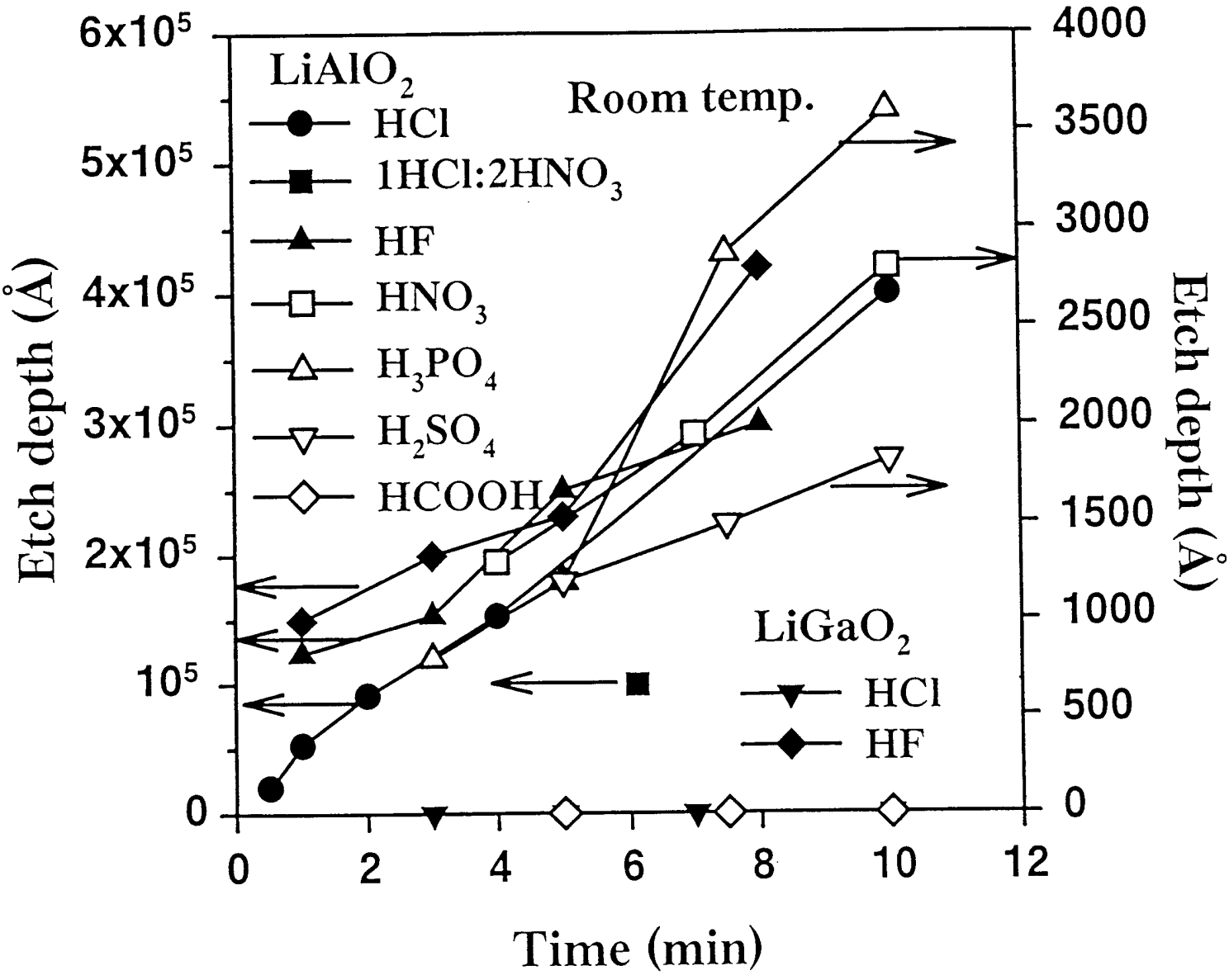
LiAlO2
Room temp.
HCl
1HCl:2HNO3
HF
HNO3
H3PO4
H2SO4
HCOOH
LiGaO2
HCl
HF
Etch depth (Å)
Etch depth (Å)
Time (min)
6x10^5
5x10^5
4x10^5
3x10^5
2x10^5
10^5
0
4000
3500
3000
2500
2000
1500
1000
500
0
0
2
4
6
8
10
12

Fig. II.1.

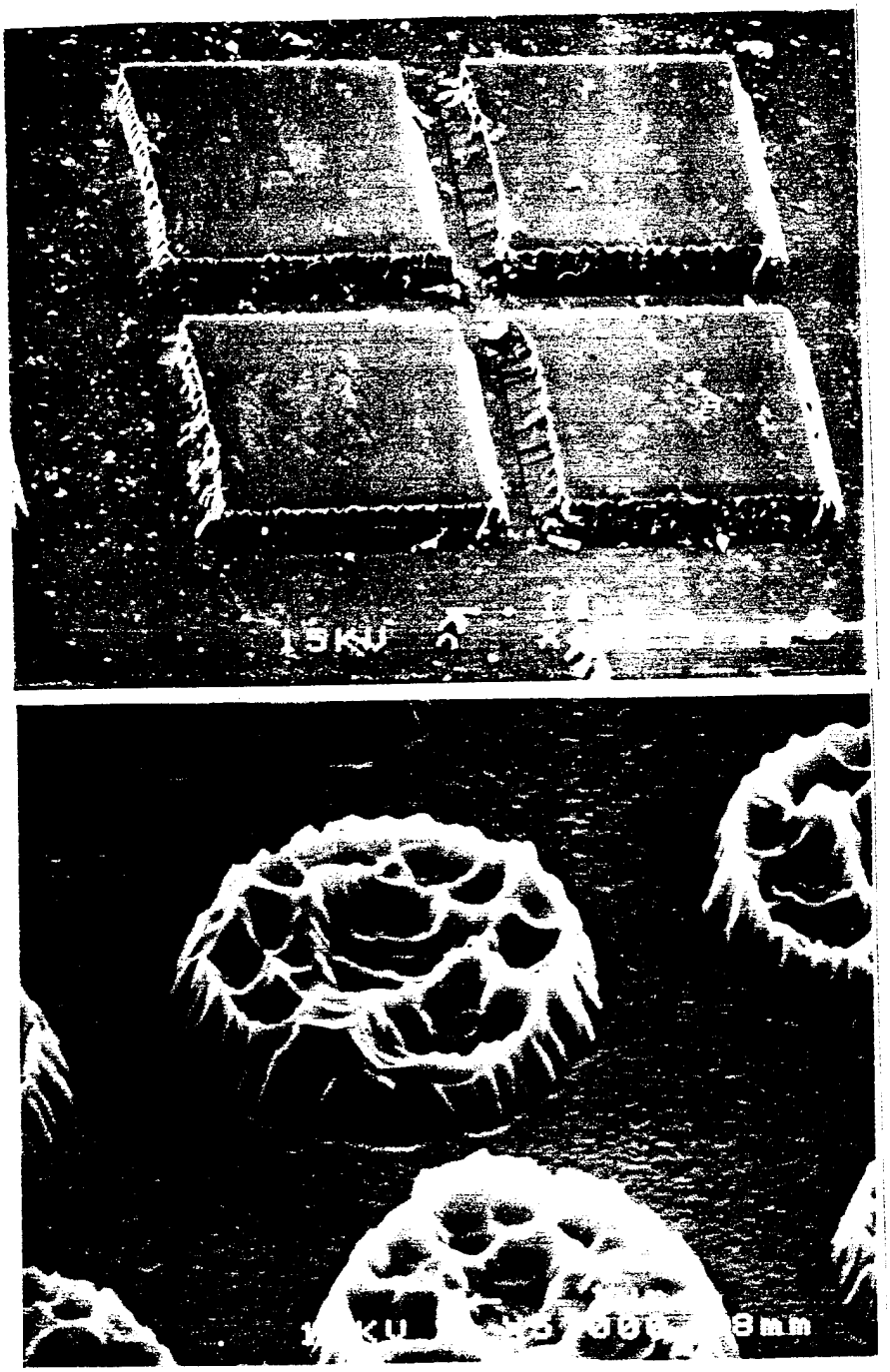

Fig. II.2.

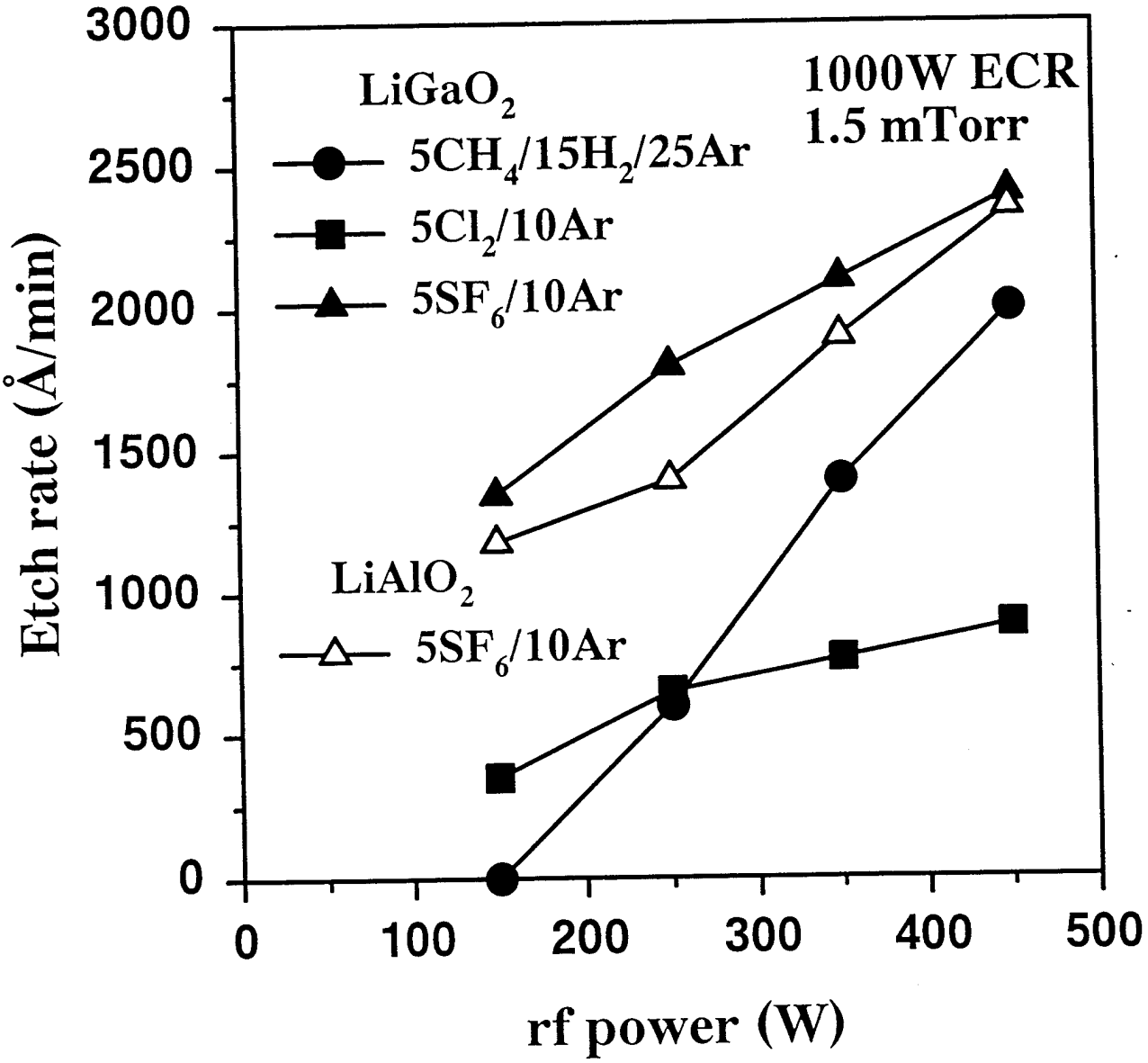
3000
2500
2000
1500
1000
500
0
Etch rate (Å/min)
LiGaO2
5CH4/15H2/25Ar
5Cl2/10Ar
5SF6/10Ar
1000W ECR
1.5 mTorr
LiAlO2
5SF6/10Ar
0
100
200
300
400
500
rf power (W)

Fig. II.3.

(similar RMS roughness for an unetched control). The high ion density under these conditions produces severe distortion of the photoresist mask, causing the resist to reticulate and leading to rough sidewalls. For these slow etching materials, dielectrics or metal masks must be employed because of their superior etch resistance compared to photoresist.

The dependence of $LiGaO_2$ and $LiAlO_2$ etch rate on microwave power at fixed pressure (1.5 mTorr) and rf power (250 W) is shown in Fig. II.4. There is only a slight increase in rate for Cl_2/Ar and CH_4/H_2/Ar at higher microwave powers, confirming that the etching is not reactant-limited since the active neutral species density increases rapidly under these conditions. By contrast the rates for both materials approximately double in the SF_6/Ar mixture between 400 and 1000 W microwave power, which is a more typical result for ECR reactors. Since the fluoride etch products are more volatile than those from the Cl_2/Ar and CH_4/H_2/Ar, an increase in ion density and fluoride radical density at high microwave powers will enhance the etch rates.

In conclusion, we have found that lithium gallate and lithium aluminate bulk wafers can be wet chemically etched in many common acid solutions with rates ranging from 150-40,000 Å/min. Chlorine, fluorine and methane-hydrogen plasma chemistries can all be employed for dry etching of both materials, with SF_6/Ar providing the fastest rates for similar plasma parameters. These processes should prove useful for patterning $LiGaO_2$ and $LiAlO_2$ substrates prior to growth of GaN and related alloys.

II.b. High Temperature Surface Degradation of III-V Nitrides

The surface stoichiometry, surface morphology and electrical conductivity of AlN, GaN, InN, InGaN and InAlN was examined at rapid thermal annealing temperatures up to 1150°C. The sheet resistance of the AlN dropped steadily with annealing, but the surface showed signs of roughening only above 1000°C. Auger Electron Spectroscopy (AES) analysis showed little change in the surface stoichiometry even at 1150°C. GaN root mean square (RMS) surface roughness showed an overall improvement with annealing, but the surface became pitted at 1000°C, at which point the sheet resistance also dropped by several orders of magnitude, and AES confirmed a loss of N from the surface. The InN surface had roughened considerably even at 650°C, and scanning electron microscopy (SEM) showed significant degradation. In contrast to the binary nitrides the sheet resistance of InAlN was found to increase by $\sim 10^2$ from the as grown value after annealing at 800°C and then remain constant up to 1000°C, while that of InGaN increased rapidly above 700°C. The RMS roughness increased above 800°C and 700°C respectively for InAlN and InGaN samples. Indium droplets began to form on the surface at 900°C for InAlN and at 800°C for InGaN, and then evaporate at 1000°C leaving pits. AES analysis showed a decrease in the N concentration in the top 500 Å of the sample for annealing ≥800°C in both materials.

Much progress has recently been made in the areas of growth, dry etching and implant isolation and doping of the III-V nitrides and their ternary alloys. This has resulted in nitride-based blue/UV light emitting and electronic devices. High temperature annealing is necessary in many of the processing steps for these devices, including activation of implanted ions, maximization of implant isolated regions or high

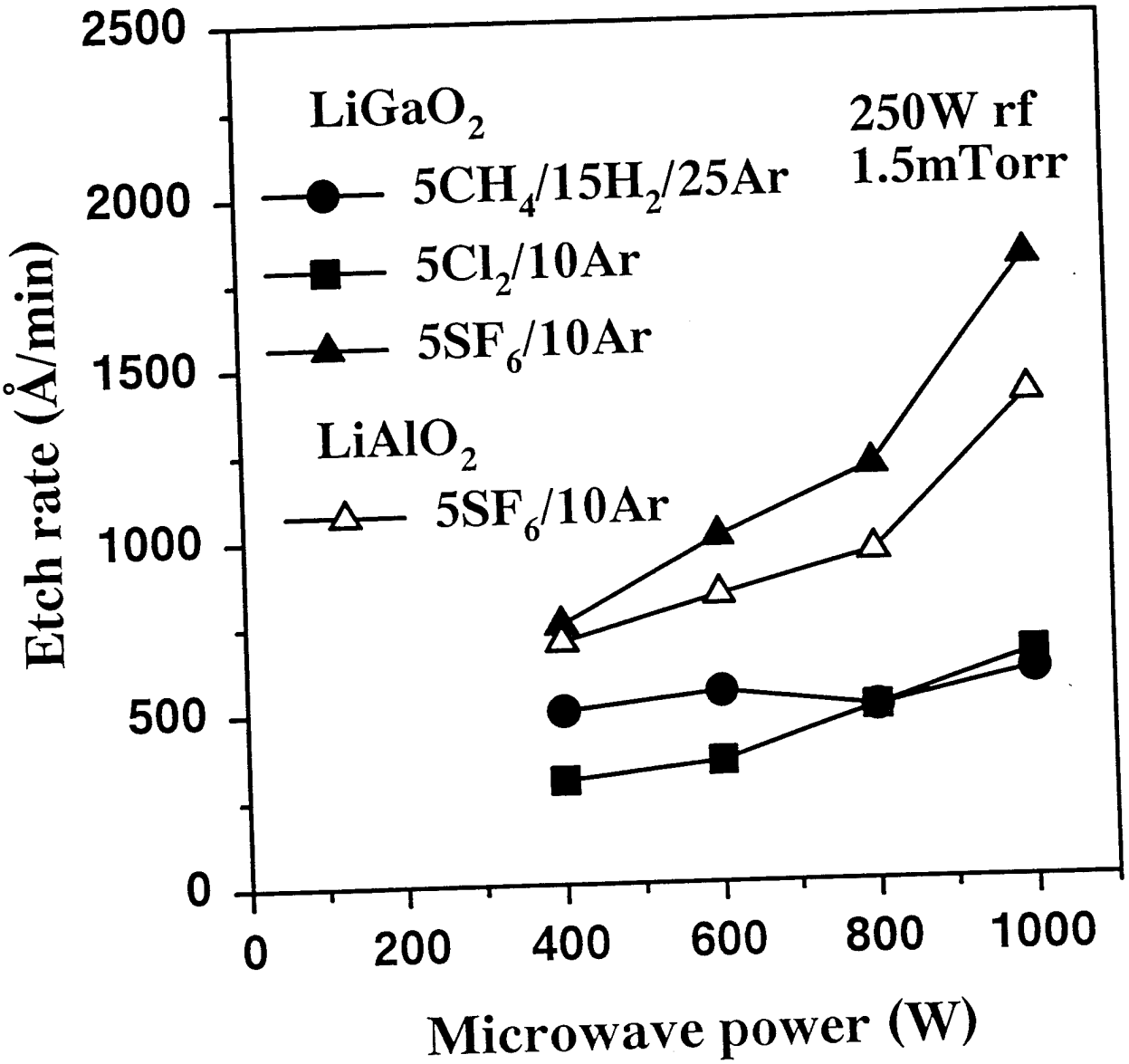
2500
2000
1500
1000
500
0
Etch rate (Å/min)
LiGaO2
5CH4/15H2/25Ar
5Cl2/10Ar
5SF6/10Ar
LiAlO2
5SF6/10Ar
250W rf
1.5mTorr
0
200
400
600
800
1000
Microwave power (W)

Fig. II.4

temperature alloying of metal contacts. A key issue is the question of surface degradation of the III-V nitrides during these high temperature anneals. A variety of authors previously published experimental and theoretical vapor pressure curves for AlN, GaN and InN.

In all of this previous work the equilibrium N_2 pressures above the solid (or solid plus liquid) have been the focus. In many process steps rapid thermal annealing (RTA) using the proximity geometry is employed, and this is a non-equilibrium situation. In this case the sample of interest is placed face-down on a substrate that can provide a group V partial pressure, and heating by tungsten-halogen lamps produces temperature ramp rates of 100 - 200°C•s^{-1}. The luminescence and surface morphologies of GaN annealed in flowing N_2 were found to improve for RTA temperatures up to 1100°C. Similar results were obtained at lower temperatures by Lin et. al. This is a common situation for lattice-mismatched systems (e.g. GaAs/Si), where post-growth or even in-situ annealing is generally found to improve structural and optical properties, provided that group V loss from the surface can be suppressed and that external impurities do not diffuse in during the anneal.

Here we report on an investigation of the thermal stability of AlN, GaN, InN, InAlN and InGaN during rapid thermal annealing. the electrical conductivity, surface morphology and surface stoichiometry have all been measured as a function of annealing temperature. The In-containing materials are found to be substantially less thermally stable than either GaN or AlN, and loss of nitrogen creates a thin n-type surface layer in all three binary nitrides.

The GaN, AlN, InN, InGaN and InAlN samples were grown using Metal Organic Molecular Beam Epitaxy (MO-MBE) on semi-insulating, (100) GaAs substrates or Al_2O_3 c-plane substrates in an Intevac Gen II system. The group-III sources were triethylgallium, trimethylamine alane and trimethylindium, respectively, and the atomic nitrogen was derived from an ECR Wavemat source operating at 200 W forward power. The layers were single crystal with a high density (10^{11} - 10^{12} cm^{-2}) of stacking faults and microtwins. The GaN and AlN were resistive as-grown, and the InN was highly autodoped n-type (>10^{20} cm^{-3}) due to the presence of native defects. InAlN and InGaN were found to contain both hexagonal and cubic forms. The $In_{0.75}Al_{0.25}N$ and $In_{0.5}Ga_{0.5}N$ were conducting n-type as grown (~ 10^{19} cm^{-3}) due to residual autodoping by native defects.

The samples were annealed in a rapid thermal anneal (RTA) system (AG 410T) face down on a GaAs substrate for 10 s at temperatures between 650 - 1150°C in a N_2 atmosphere. We employed GaAs in the hope that decomposition of As from these substrates might help to prevent nitrogen loss from the nitride samples. The sheet resistance was measured at room temperature on a Van der Pauw Hall system with InHg alloyed contacts (300°C, 3 min) on the corners. An Atomic Force Microscope (AFM), operated in tapping mode with Si tips, was used to measure the root mean square (RMS) roughness of the samples. The surface morphology was also examined with a scanning electron microscope (SEM). Energy dispersive X-ray spectrometry (EDAX) was used to analyze the surface composition of InAlN. Auger electron spectroscopy (AES) was used to investigate near-surface stoichiometry before and after anneal.

The sheet resistance normalized to the as grown value for all of the nitride samples is shown in Fig. II.5 as a function of annealing temperature. The values for the GaN, AlN and InN are found to drop by approximately three orders of magnitude with annealing, up to 900°C. The material becomes strongly n-type in all cases, even in the GaN and AlN which were resistive as grown. The sheet resistance for AlN continues drop steadily with anneal temperature until 1100°C. As will be shown below, AlN shows only a small loss of N from the surface as determined by AES. However the electrical measurements are more sensitive to small changes in the composition than the Auger. Here we believe the N vacancies created by the loss of N from the surface are creating shallow donors. This agrees with the theoretical prediction of Maruska and Tietjen. The actual values of sheet resistance for AlN are much higher than the GaN up to 900°C, and significantly higher than InN at all temperatures. The data in Fig. II.5 is in agreement with the melting point and vapor pressure curves for these materials. AlN is predicted to be stable under N_2 gas up to ~2500°C, and to melt at ~ 3700°C at atmospheric pressure. GaN is predicted to melt at ~3000°C and InN at only ~2400°C and to degrade at 600°C AES has confirmed loss of N from the annealed GaN sample which would suggest that N vacancies are contributing to the conductivity. Above 900°C Ga vacancies in the GaN may be creating compensating shallow acceptors, thus causing the sheet resistance to level off. We also may be getting Ga or N antisite defects which form deeper traps. At 1150°C the sheet resistance for the GaN drops sharply indicating that N is being lost at a much greater rate than the Ga. Groh et. al. showed loss of nitrogen beginning at 710°C in vacuum annealed GaN, with significant loss at ≥ 980°C. The sheet resistance for the InN drops steadily over the temperature range, which correlates to the problems of nonstochiometry in InN. The large size difference between the N and In make the material less stable.

The sheet resistance for InGaN and InAlN on the other hand, increases with annealing. The InAlN sheet resistance increases by 10^2 from the value for the as grown material when annealed at 800°C. Its resistance then remains constant to 900°C, and then decreases slightly at 1000°C. For InGaN the sheet resistance remains constant up to 700 °C and then increases rapidly with increasing temperature. This suggests that simple N vacancies are not the cause of the residual n-type conductivity in these samples since at the highest temperatures we are losing N from the surface, as described below. However these samples become less conducting, suggesting creation of compensating acceptors or annealing of the native donors is occurring. It is likely, in contrast to the binary nitrides, that the V_N have several different energy levels in the ternaries because of the differences in strength between In-N and Ga-N bonds. Some of these may be creating a deep acceptor which compensates the shallow donors, or a deep level electron trap, making the material more resistive. There could also be the presence of compensating V_{Ga} or V_{In}-related defects, which might be easier to form in ternaries because of different sizes and bond strengths of the In and Ga. Finally it is possible that at least some of the conductivity in the ternaries is due to carbon-related donors, and subsequent annealing might produce carbon self-compensation, as in other III-V's. At this point we cannot be more precise regarding the differences between the binaries and the ternaries and this is under close examination.

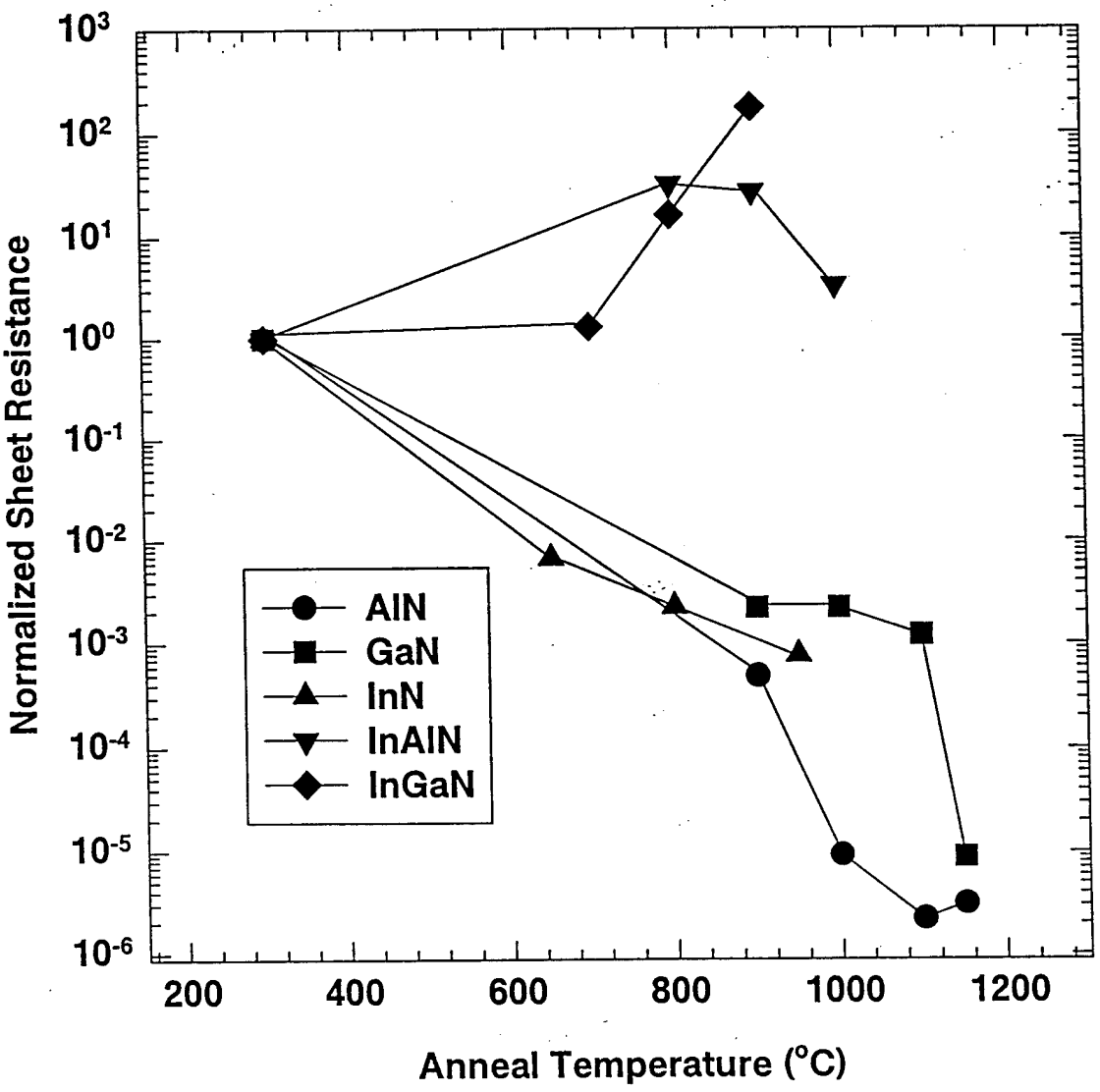
Normalized Sheet Resistance
10^3
10^2
10^1
10^0
10^-1
10^-2
10^-3
10^-4
10^-5
10^-6
200
400
600
800
1000
1200
Anneal Temperature (°C)
AlN
GaN
InN
InAlN
InGaN

Fig. II.5.

The RMS data normalized to the as grown roughness as a function of anneal temperature is shown in Fig. II.6 for AlN, GaN and InN. The AlN is still smooth at 900 °C, but becomes quite rough at 1000°C. Further surface reconstruction continues at higher annealing temperatures. At 1150°C the sample becomes smooth again-in fact slightly smoother than the as grown sample. GaN shows no roughening, becoming smoother with annealing due to defect annealing and surface reconstruction. InN on the other hand is a factor of two rougher than for as grown samples at 650°C, indicating the weaker bond strength of this material.

In Fig. II.7 the RMS roughness for InAlN and InGaN are shown as a function of rapid thermal anneal temperature. We see that the InAlN remained smooth until 800°C, and at 900°C has increased an order of magnitude in roughness. At 1000°C the RMS roughness returns to a value close to that of the value for the as grown material. We found this to be a result of In droplets forming on the surface above 800°C and then evaporating above 900°C. The InGaN surface was unchanged at 700°C, with the roughness increasing above that temperature.

In Fig. II.8 SEM pictures of AlN, GaN and InN are shown for as grown, (left) and annealed (right) samples. AlN has no visible surface damage, even at 1150°C. GaN has become slightly rough and pitted at 1000°C, and InN has degraded at 800°C to a large extent, showing pits and various defect structures. InAlN is shown in Fig. II.9 for as grown (top), 900°C anneal (middle) and 1000°C anneal (bottom). The unannealed surface is reasonably smooth with small particulates. At 900°C In droplets are seen to form on the surface as determined by EDAX. At 1000°C the In evaporated off the surface leaving dark, In deficient areas. This accounts for the reduced RMS roughness of the 1000°C annealed sample. In droplets began to form on the surface of the InGaN samples at 800 °C and continue to grow at 900°C. Confirmation that we are indeed observing In droplets comes from direct chemical identification by EDAX which showed a reduced Ga/In ratio around the precipitate relative to the background on which the precipitate sits.

In Fig. II.10 through II.12 the AES depth profiles and surface scans for AlN and GaN, as grown and annealed at 1150°C are shown. On all the samples the surface was contaminated with oxygen from a native oxide and adventitious carbon because of exposure to ambient when transferring the material from the annealing furnace to the AES analysis chamber. After the 1150°C anneal of AlN (Fig. II.10), less C, O and Al are found on the surface compared to the as grown sample. Ga was found to have diffused into the top 50 Å of the material from the proximity wafer used during annealing. The N appears to have been lost only from the top 100 Å or so from the surface as a result of annealing, showing the excellent thermal stability of this material.

In Fig. II.11 and II.12 the AES depth profiles and surface scans for GaN as grown and annealed at 1150°C are shown. For these samples the oxygen at the surface of the annealed sample has decreased, but the C content of the surface has increased, as has that of the Ga and N. The proximity cap worked well for the Ga component. The Ga/N ratio measured by raw AES counts increased from 1.73 on the as-grown samples to 2.34 after 1150°C annealing, indicating that nitrogen was indeed lost from the surface. Similar data is shown in Fig. II.13 and II.14 for InAlN and InGaN as grown and annealed at 1000°C and 800°C respectively. Both materials show a definite decrease in the amount of N at the

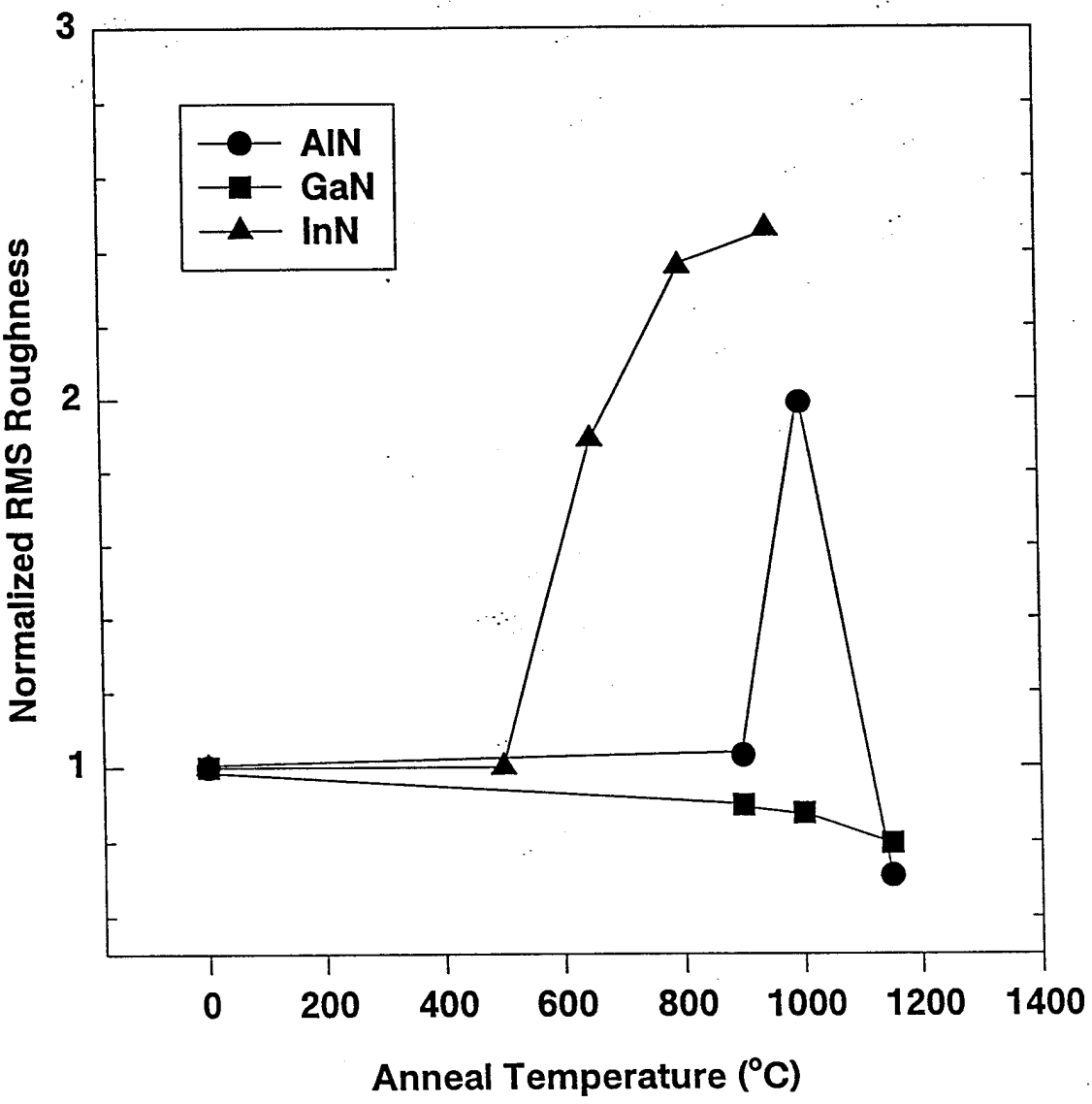
AlN
GaN
InN
Normalized RMS Roughness
3
2
1
0
200
400
600
800
1000
1200
1400
Anneal Temperature (°C)

Fig. II.6.

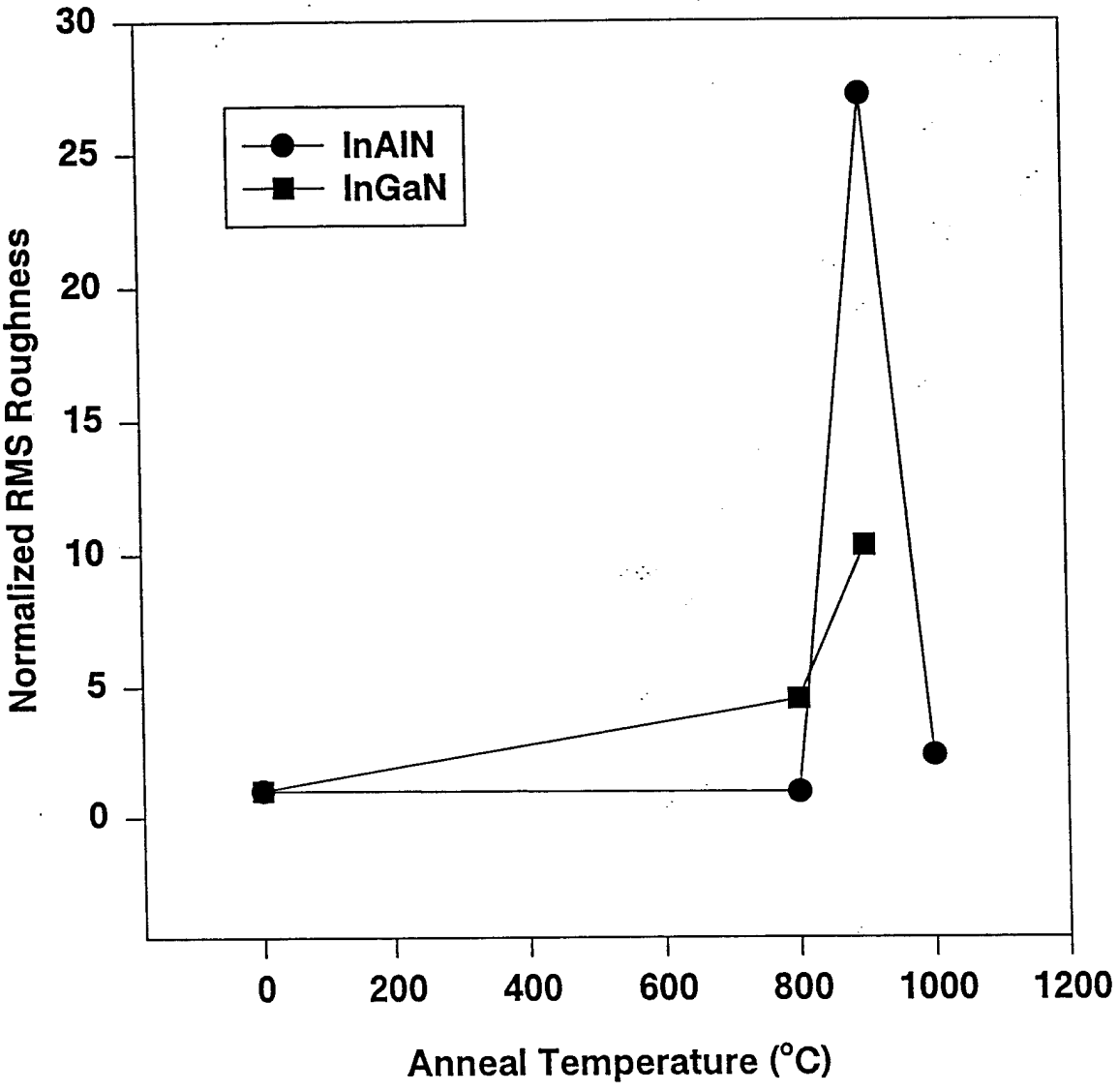
30
25
20
15
10
5
0
Normalized RMS Roughness
InAlN
InGaN
0
200
400
600
800
1000
1200
Anneal Temperature (°C)

Fig. II.7.

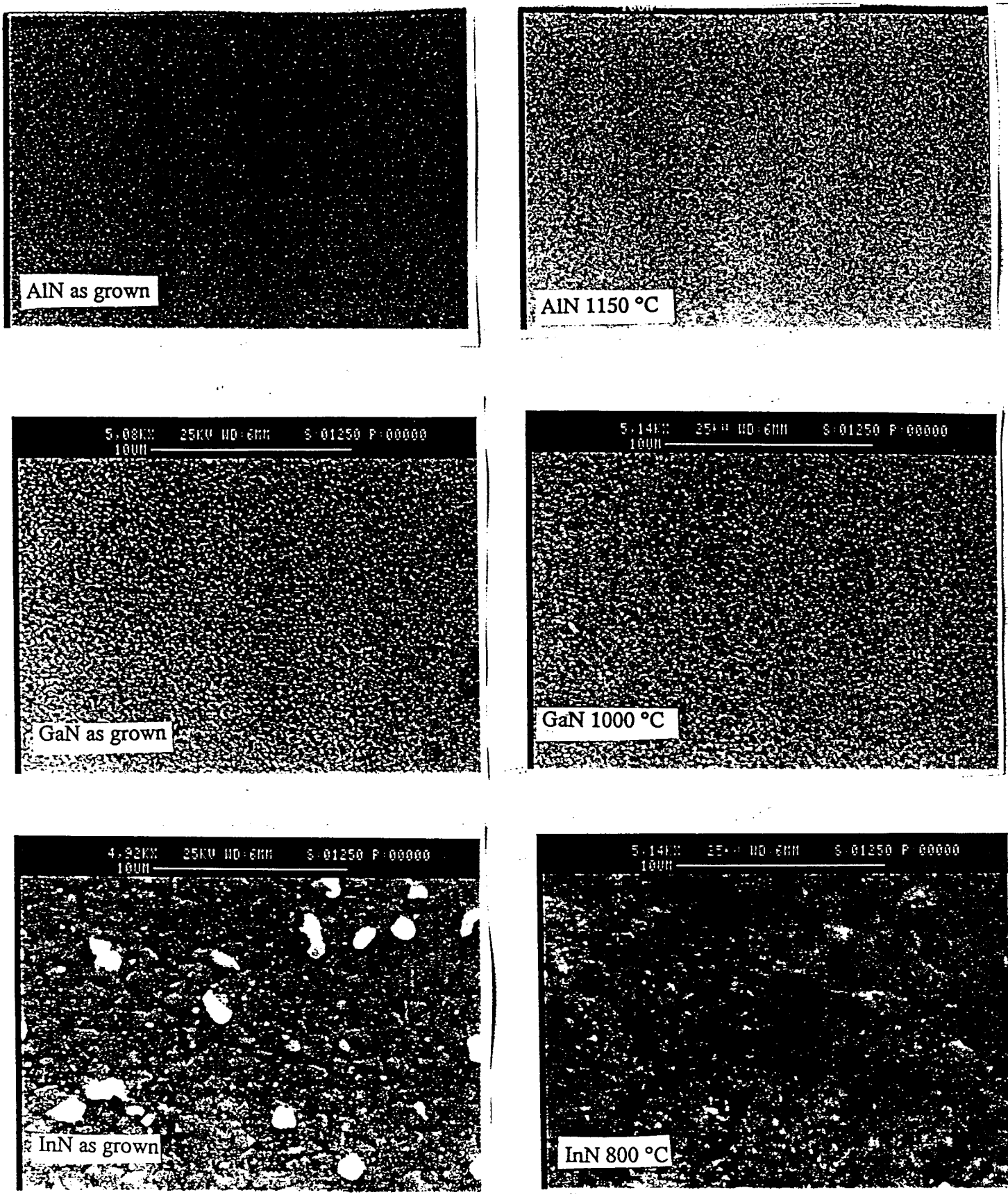
AlN as grown
AlN 1150 °C
5.08KV 25KV WD:6MM S:01250 P:00000
10UM
GaN as grown
5.14KV 25KV WD:6MM S:01250 P:00000
10UM
GaN 1000 °C
4.92KV 25KV WD:6MM S:01250 P:00000
10UM
InN as grown
5.14KV 25KV WD:6MM S:01250 P:00000
10UM
InN 800 °C

Fig. II.8.

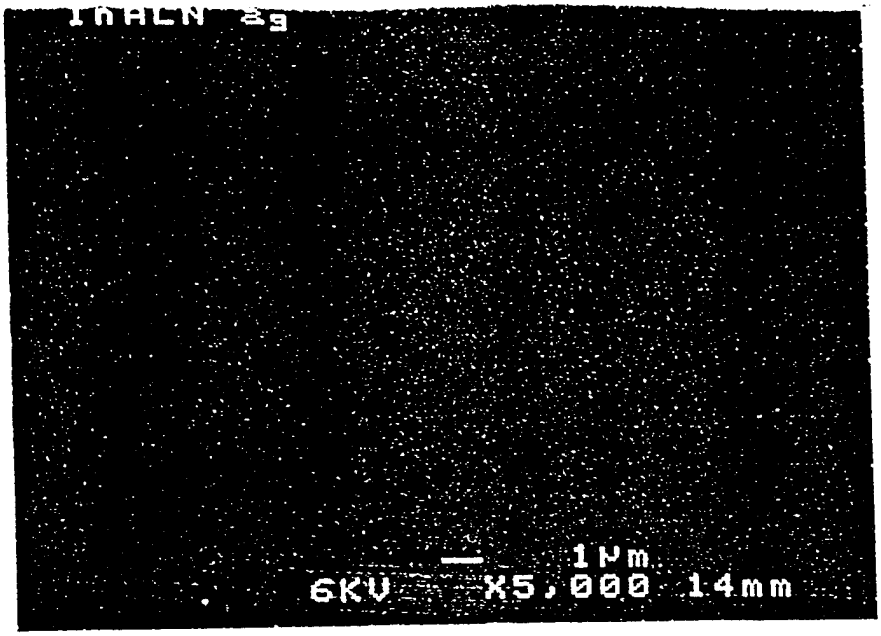
InALN 29
1μm
6KV X5,000 14mm

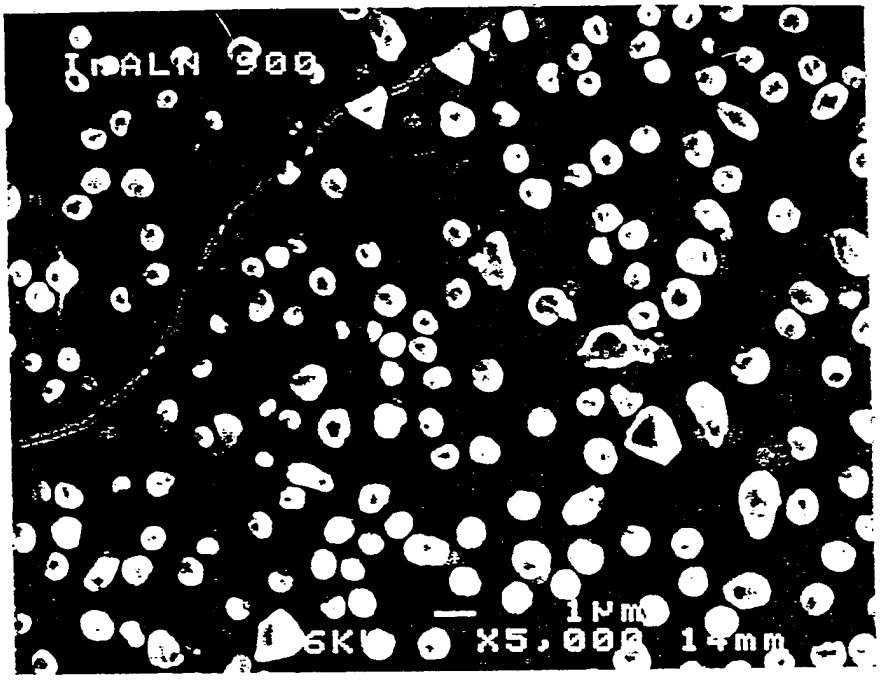
InALN 900
1μm
6K X5,000 14mm

Fig. II.9.

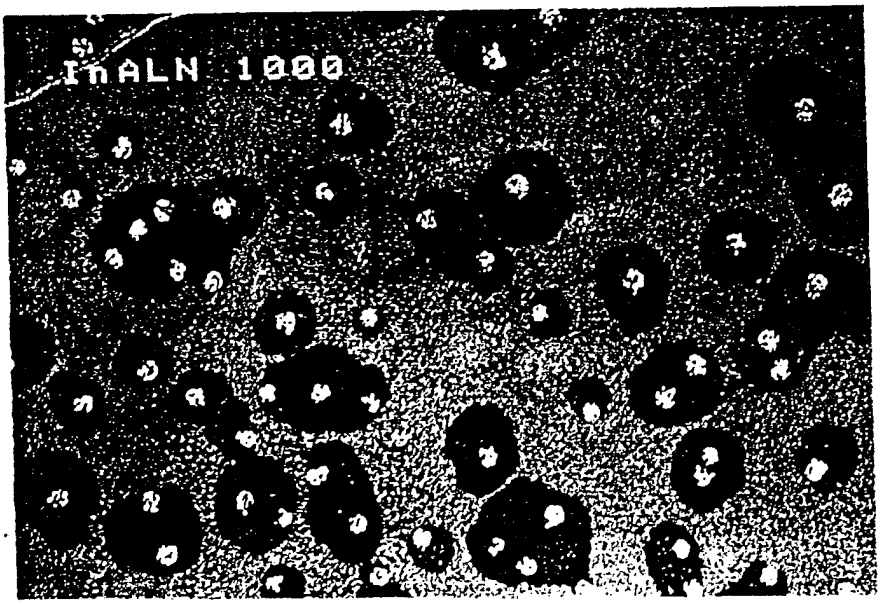
InALN 1000

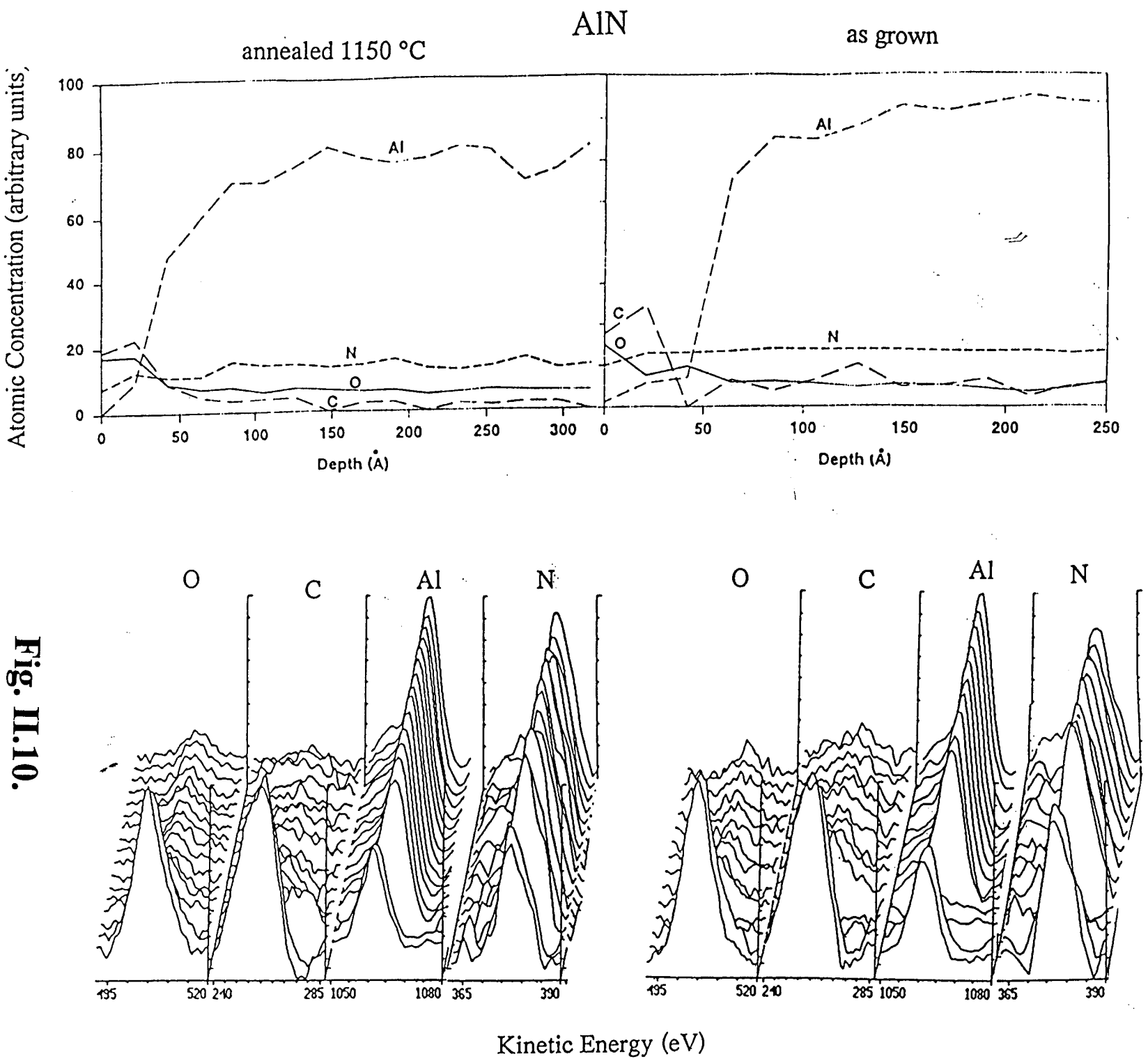
AlN
annealed 1150 °C
as grown
Atomic Concentration (arbitrary units)
Al
N
O
C
Depth (Å)
O
C
Al
N
Kinetic Energy (eV)

Fig. II.10.

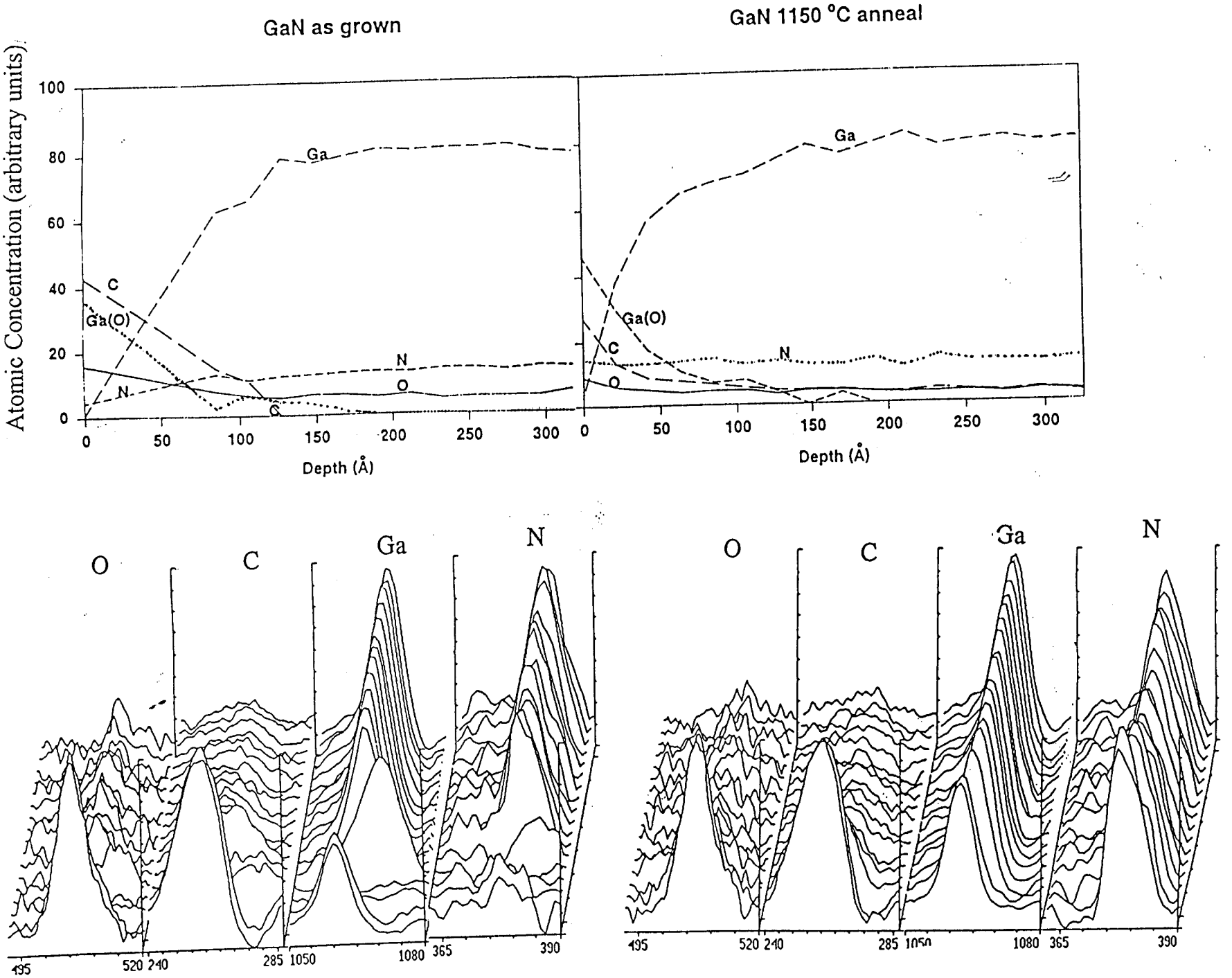
GaN as grown
GaN 1150 °C anneal
Atomic Concentration (arbitrary units)
Depth (Å)
Ga
C
Ga(O)
N
O
O
C
Ga
N
Kinetic Energy (eV)

Fig. II.11.

GaN

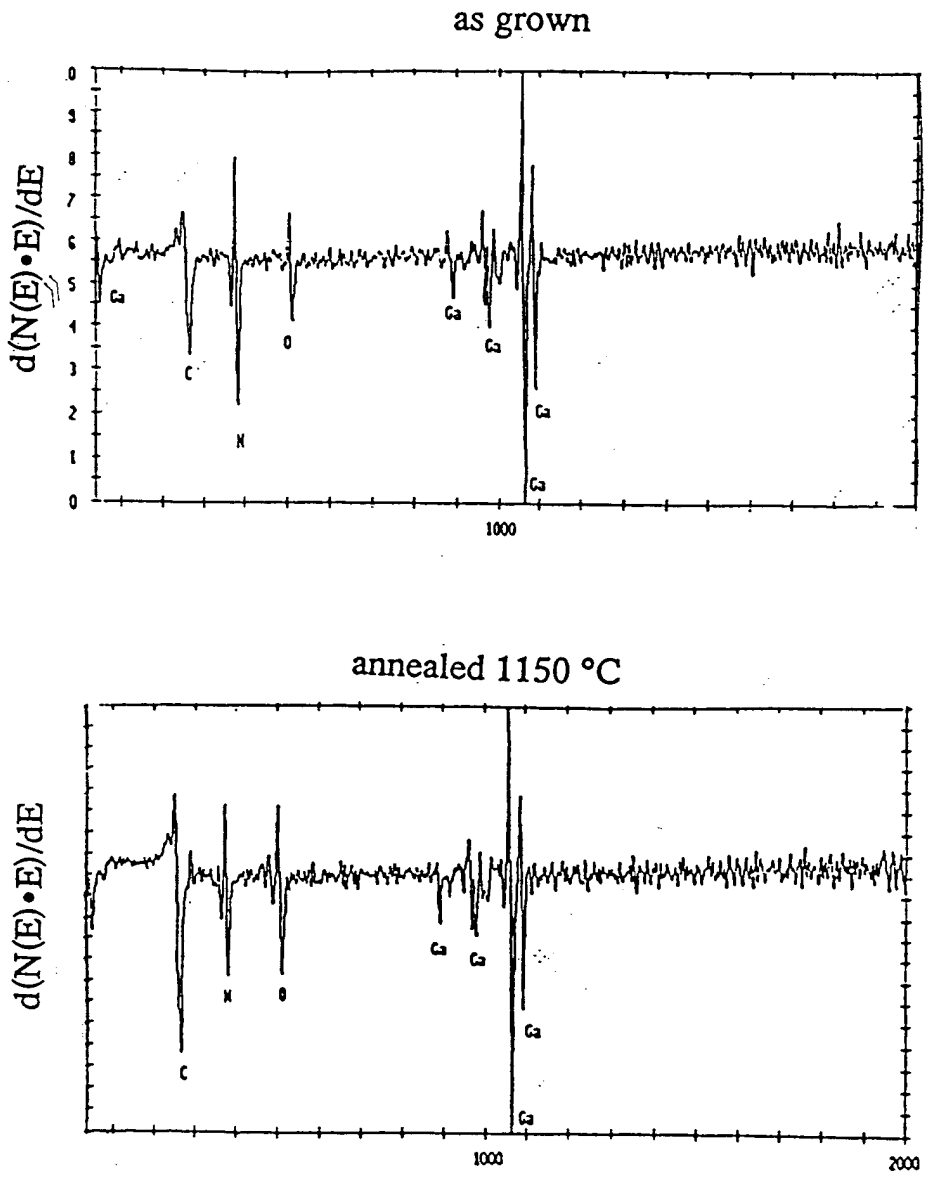
as grown
d(N(E)•E)/dE
Ga
C
N
O
Ga
Ga
Ga
Ga
1000
annealed 1150 °C
d(N(E)•E)/dE
C
N
O
Ga
Ga
Ga
Ga
1000
2000

Fig. II.12.

InAlN

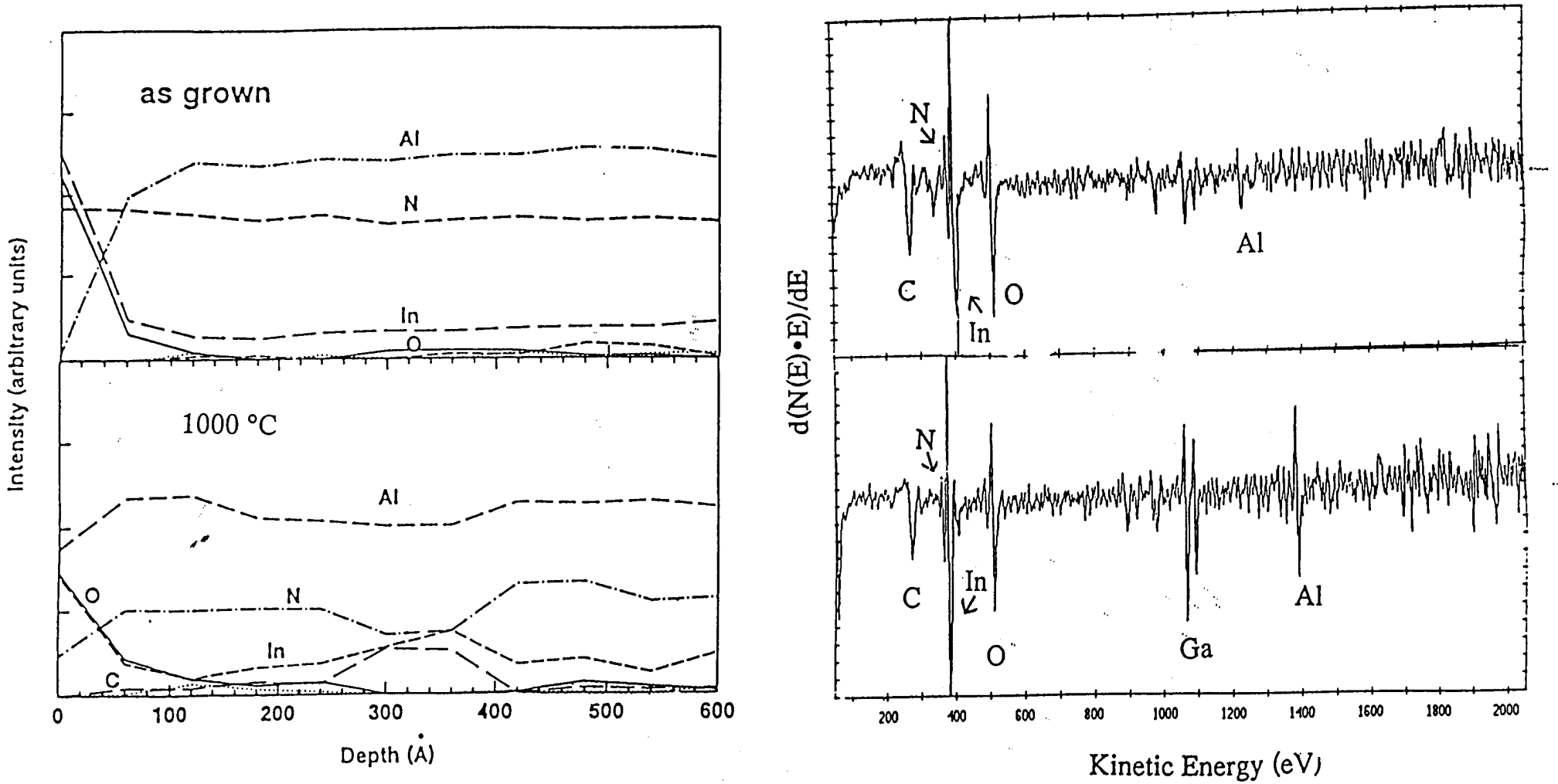

Fig. II.13.

InGaN

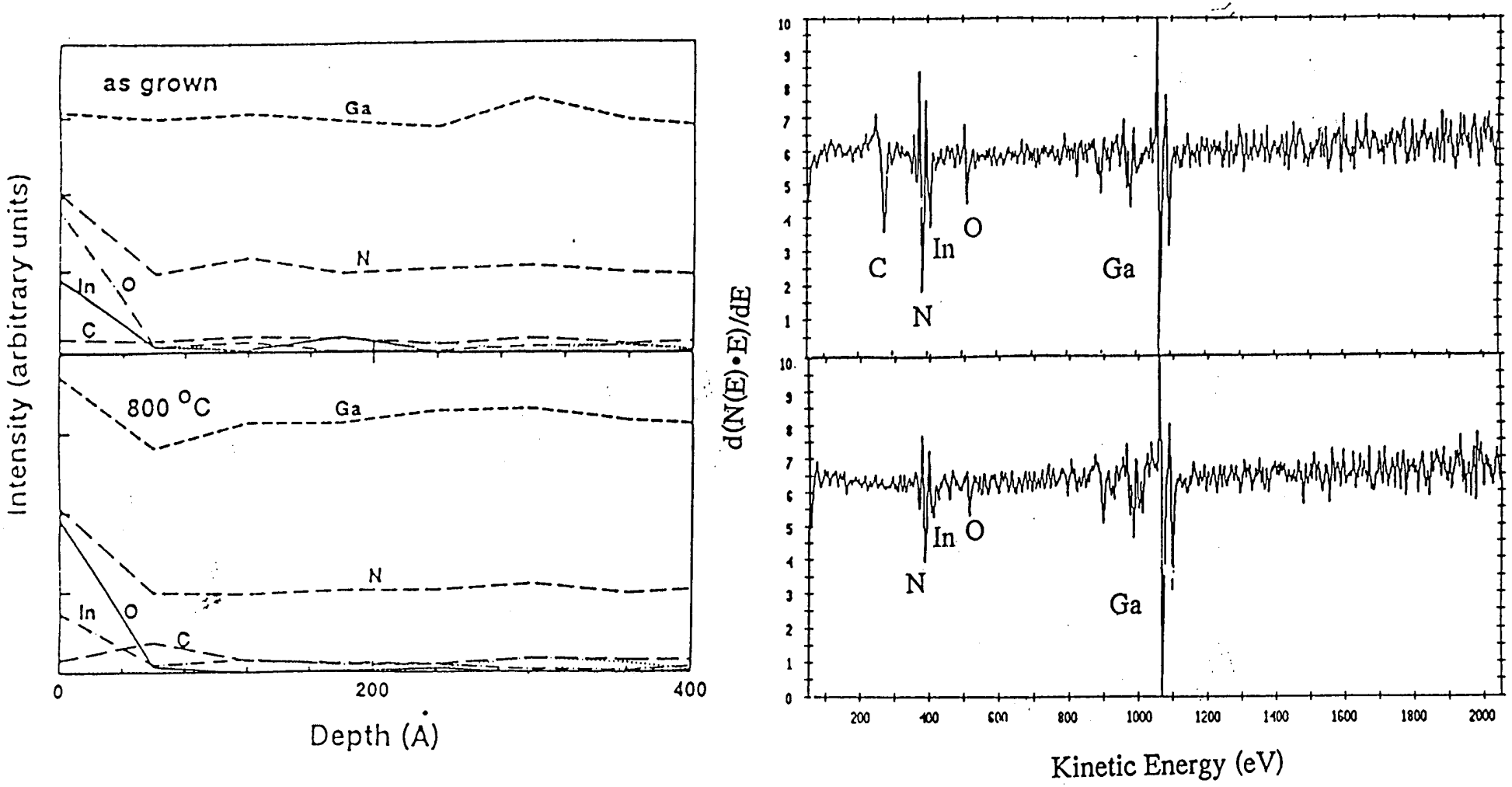

Fig. II.14.

surface of the samples after anneal. In the case of InGaN there was also a reduction in In, which could be related to the changes in the electrical properties. The amount of N, C and O are also seen to decrease at the surface. For InAlN the amount of Al increased at the surface, and both samples experienced Ga diffusion in the first 50 Å or so from the proximity cap. The surfaces of all the samples show a loss of N, consistent with the SEM, AFM and EDAX results discussed above.

The III-V nitrides are thermally stable to relatively high temperatures. AlN and GaN remain smooth and stochiometric at 1000°C, InAlN and InGaN up to 800°C, and InN up to 600°C. Above these temperature capping is necessary to prevent the loss of N and, sometimes, In. Consistent with the predicted melting temperatures and thermal stabilities of the nitrides, we found AlN to be somewhat more stable than GaN, and much more stable than InN. InAlN was found to be more stable than InGaN, as expected from a consideration of the binary component N_2 vapor pressures. AlN may prove to be a good capping material for the other nitrides, because of its high stability and the fact that it can be selectively removed by wet etching in KOH based solutions.

III. Ohmic Contacts to p-GaN (Jeff Trexler and Paul Holloway)

Studies continued this quarter using the ohmic contact metallizations Au/Ni, and Au/C/Ni on p-GaN, along with new attempts to form ohmic contacts using Pd and Cr in place of Ni in the previous contact schemes. All contacts were deposited by electron beam evaporation with thicknesses of 1000Å Au, 100Å C, and 500Å Ni or Pd. Contacts were generally heat treated up to 600°C for 5, 15 and 30 minutes in flowing nitrogen with current-voltage (I-V) measurements being taken after each anneal. Auger electron spectroscopy (AES) was performed on many of the samples to determine interfacial reactions between the contact metals and the underlying GaN.

The Au/Ni and Au/C/Ni contacts were rectifying as-deposited and exhibited nearly linear I-V data after heating to 400°C for 5 minutes. Upon heating to 600°C both contact schemes yielded linear I-V curves with a lower resistance for the Au/Ni contacts than for the Au/C/Ni. AES data showed evidence of Ni diffusion into the p-GaN matrix upon heat treatment. The Ni also diffuses through the Au layer to the surface where it has been shown to form a NiO_x layer. It is believed that the formation of this NiO_x is providing the driving force for the regrowth of a highly doped GaN layer which has been previously postulated. The introduction of the C layer into the contact scheme was intended to increase the carrier concentration in the near-surface region of the GaN, thus lowering the resistance. The higher resistance of the C containing contacts may be due to deposited interfacial carbon being bonded in a ring structure as opposed to a chain structure from adventitious contaminant carbon. The latter bonding form of C is preferable for doping.

It has been shown that Ni will react with GaN to a certain extent, but there are concerns that this reaction does not proceed to a deep enough level into the GaN to allow for the increased carriers to overcome the depletion distance in the semiconductor. Thus, investigations have been initiated to find a metal to replace Ni in the contact scheme.

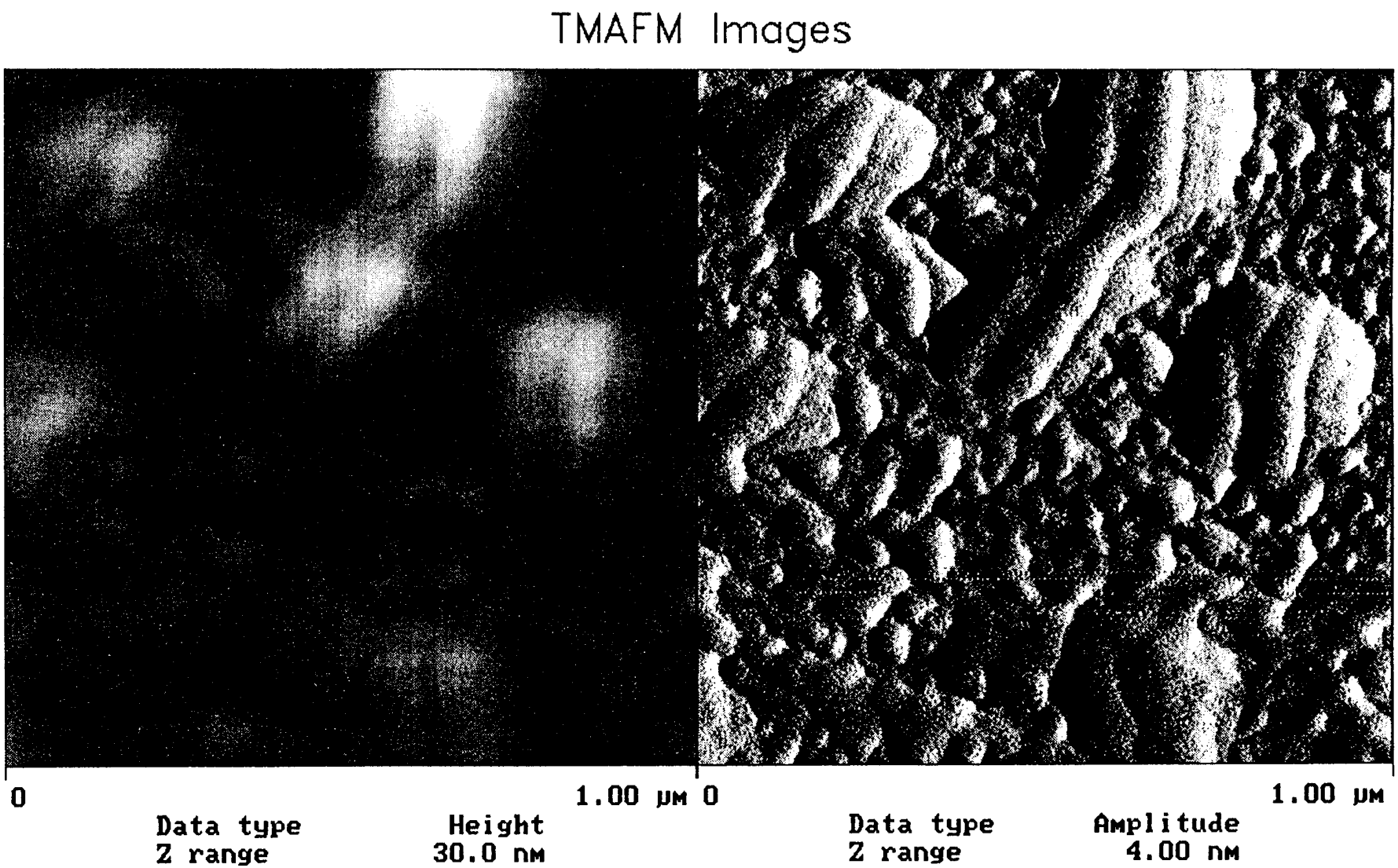

Fig. IV.1a. 1 Atomic force microscopy image of $LiGaO_2$ substrate

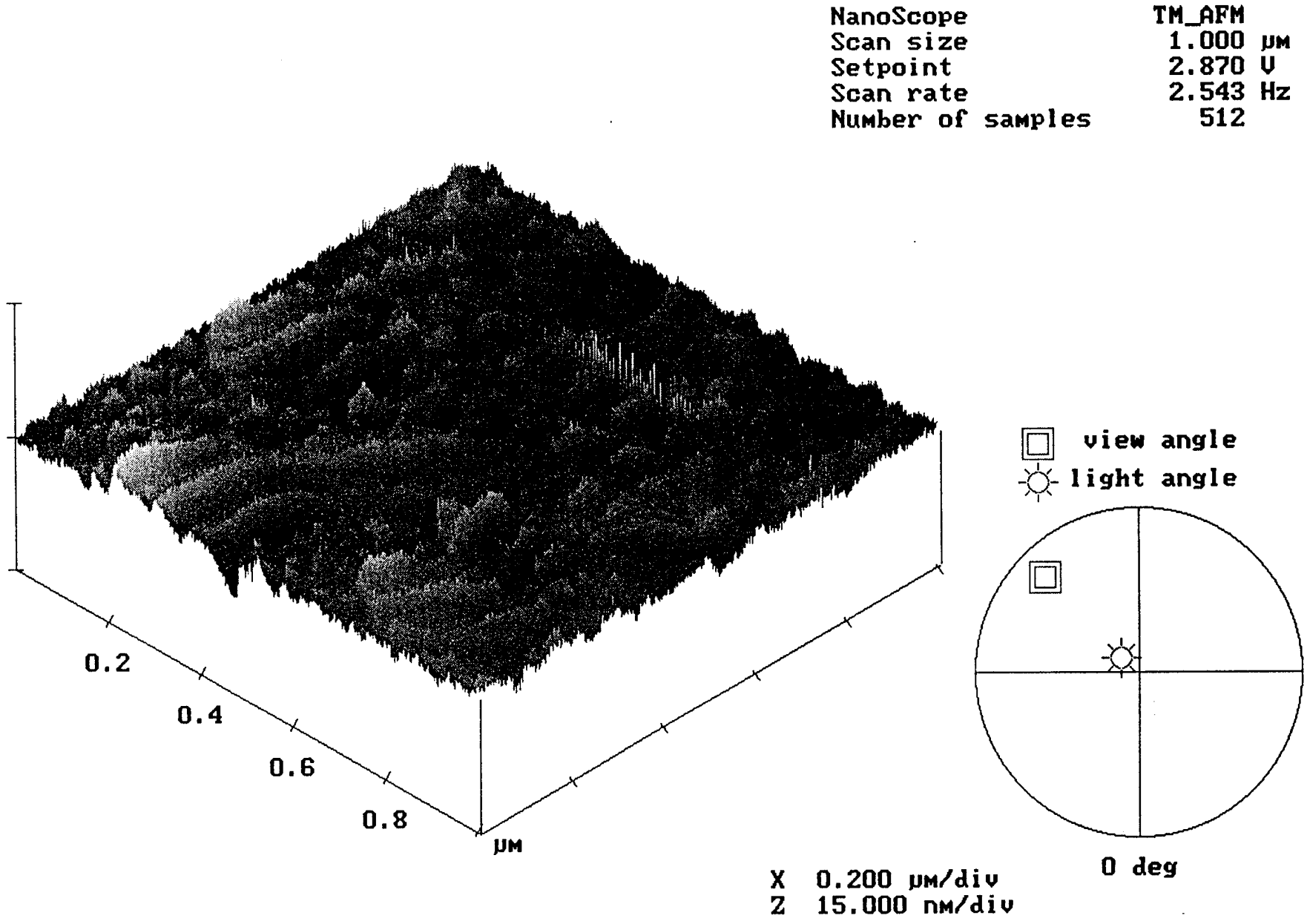

Fig. IV.1b. 3-Dimentional view of the $LiGaO_2$ substrate surface

Table IV.1. Typical growth conditions and HRXRD results

Substrates	(001) $LiGaO_2$	(110) $LiAlO_2$	(0112) r- Al_2O_3
Precursors	Triethylgallium (TEGa) Ammonia (NH_3)	Triethylgallium (TEGa) Ammonia (NH_3)	Triethylgallium (TEGa) Ammonia (NH_3)
Carrier gas	Hydrogen (H_2) Nitrogen (N_2)	Hydrogen (H_2) Nitrogen (N_2)	Hydrogen (H_2) Nitrogen (N_2)
V / III Ratio	3320 to 4880	3320 to 4880	3320 to 4880
Substrate Temp.	500 - 850 °C	500 - 850 °C	500 - 850 °C
Reactor Pressure	76 - 130 Torr	76 - 130 Torr	76 - 130 Torr
Flow Rates, sccm	TEGa: 50 NH_3: 1500 - 2100	TEGa: 50 NH_3: 1500 - 2100	TEGa: 50 NH_3: 1500 - 2100
Growth Rate	0.40 - 0.73 μm/h	0.40 - 0.73 μm/h	0.40 - 0.73 μm/h
HRXRD (2-axis) FWHM, arc sec H_2 carrier gas N_2 carrier gas	 4239.1 - 4482.8 21.6 - 73.3	 4347.8 - 4386.0 2631.6 - 5785.7	 - 39.5

a significant difference in the quality of the GaN films.

The films grown at a substrate temperatures 500 - 700 °C using H_2 as a carrier gas exhibited the granular nature of GaN films (Fig. IV.2a-b: SEM magnification x15,000). A HRXRD rocking curve measurements exhibits a FWHM of from 4240 to 4680 arc sec for each of the three types of substrates. A low temperature buffer layer was not grown in these runs. The poor structural qualities evidenced by the large FWHM values in the rocking curve was not surprising. In addition to the absence of the usual buffer layer, the growth temperature was considerable below the value typically used (~1050°C). Thus poor nucleation, lack of sufficient surface mobility and a reduced surface site exposure lead to poor quality material. In contrast to this result, GaN was grown under similar conditions, but replacing H_2 with N_2 as the carrier gas. A remarkable improvement in the structural quality of the film was observed on the $LiGaO_2$ and α-Al_2O_3 substrates.

At a deposition temperature T = 850 °C on a $LiGaO_2$ substrate with N_2 as a carrier gas,the only reflection observed was from the (0002) GaN plane. Fig. IV.3 shows the X-ray diffraction pattern of 0.5 μm GaN film grown directly on (001) $LiGaO_2$. Both the (0002) peak at $2\theta = 34.975°$ and the (0004) peak at $2\theta = 73.135°$ were observed. This is consistent with (0001) hexagonal GaN grown epitaxially on (001) $LiGaO_2$. The FWHM value of (0002) GaN peaks (Fig. IV.4a-d) are shown in Table IV.2. The FWHM value for $LiGaO_2$ substrate on double axis was 84.4 arc sec.

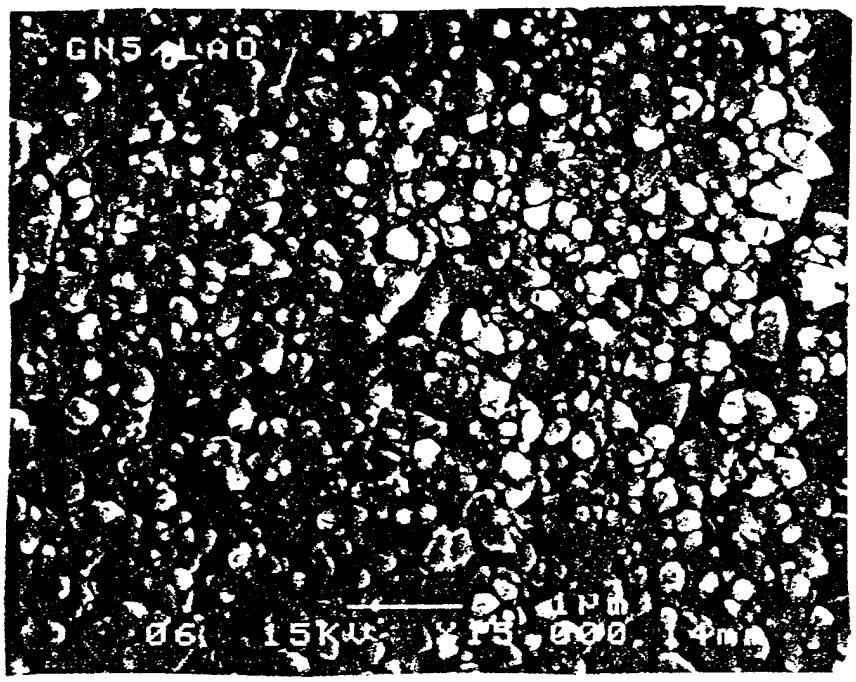

GaN/$LiAlO_2$

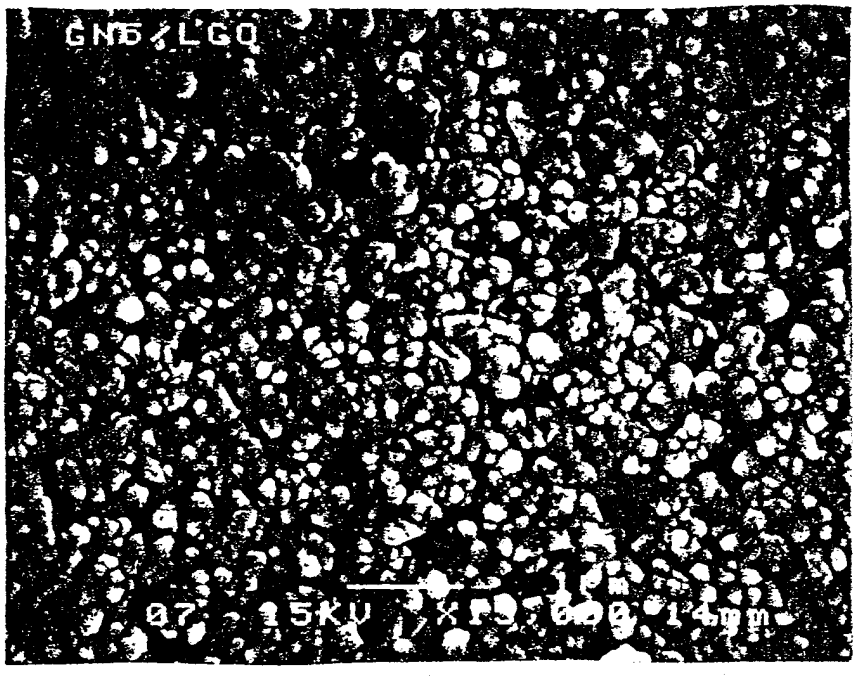

GaN/$LiGaO_2$

Fig. IV.2a. SEM image of GaN films grown on $LiGaO_2$ and $LiAlO_2$ substrates H_2 carrier gas, T = 600 C°, film thickness 0.50 μm (x 15 000)

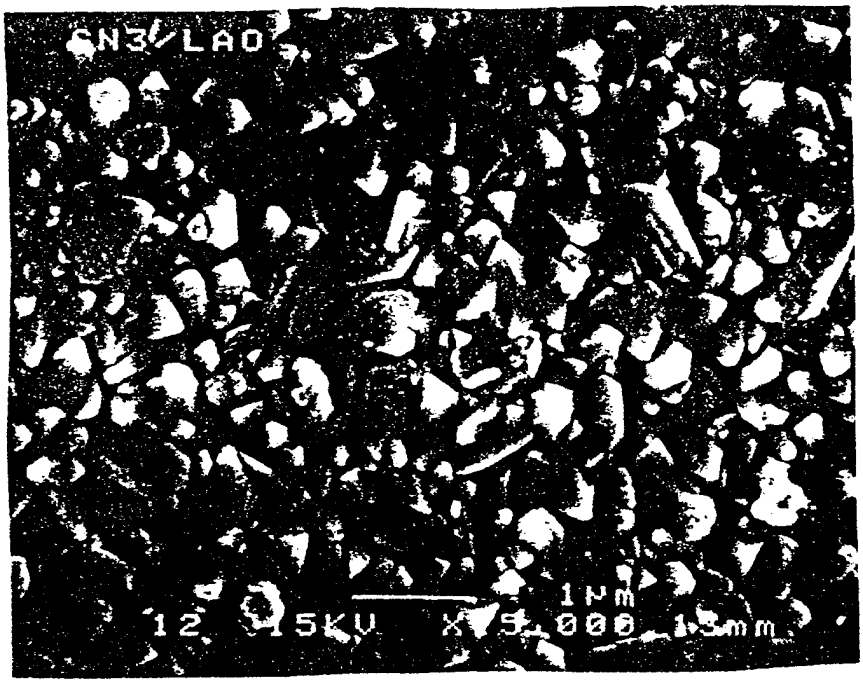

$GaN/LiAlO_2$

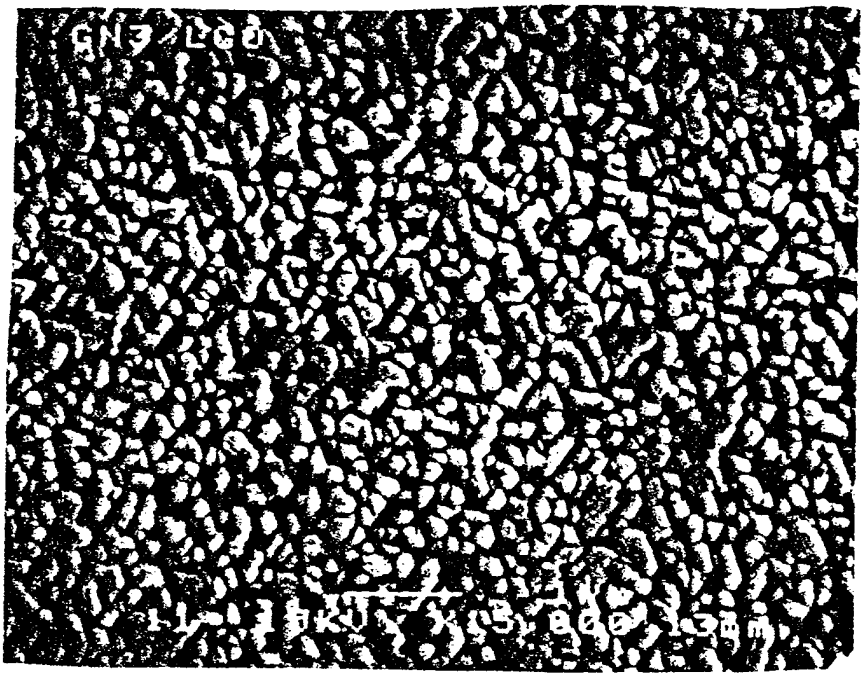

$GaN/LiGaO_2$

Fig. IV.2b. SEM image of GaN films grown on $LiGaO_2$ and $LiAlO_2$ substrates H_2 carrier gas, T = 650 C°, film thickness 1.4 μm (x 15 000)

Fig. IV.3. LRXRD GaN/$LiGaO_2$
T = 850 °C, films thickness 0.5 μm, N_2 carrier gas

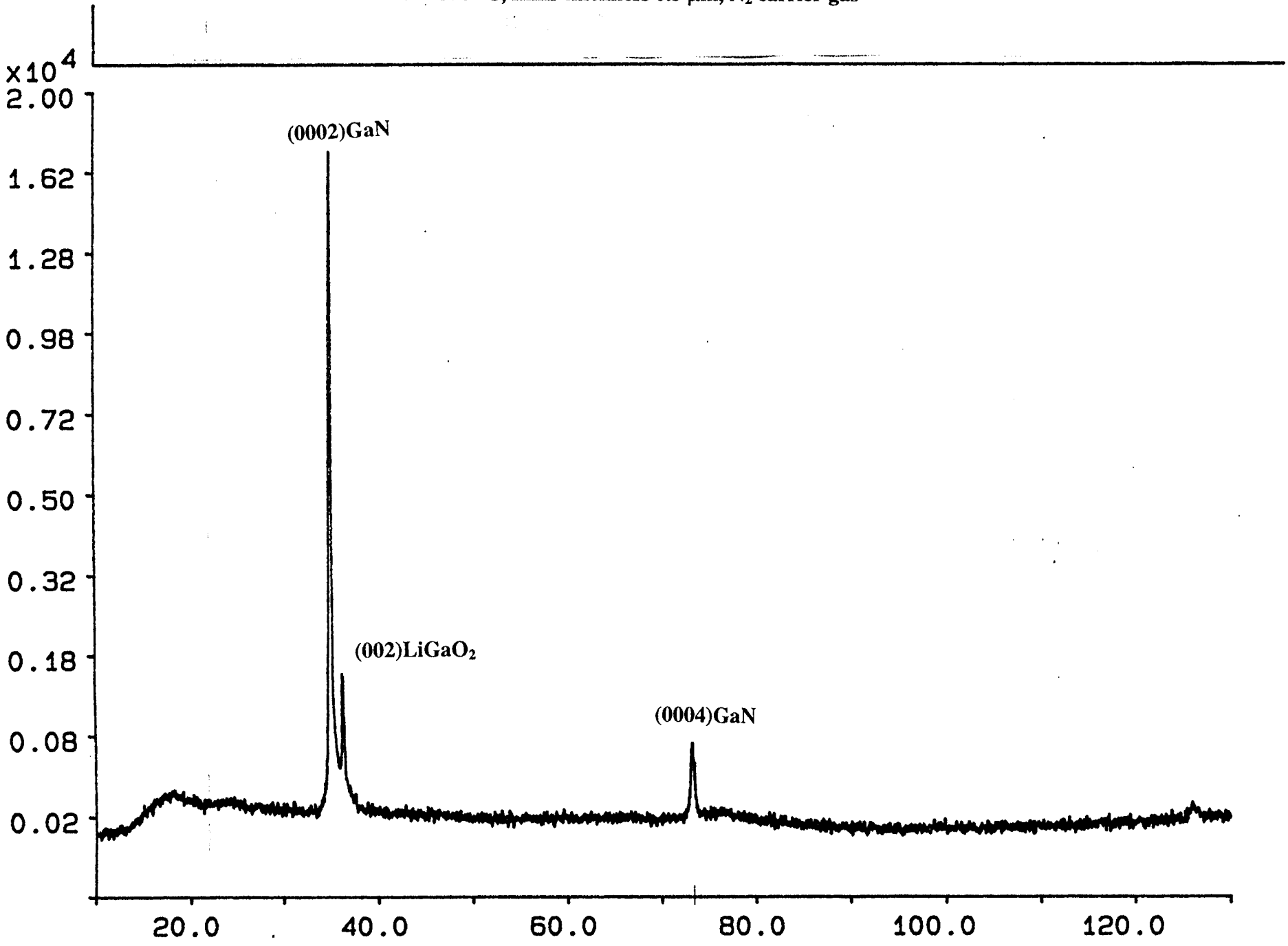

Fig. IV.4a. HRXR diffraction (double axis) GaN/$LiGaO_2$
omega / 2θ scan
T = 850 °C, film thickness 0.5 μm, N_2 carrier gas

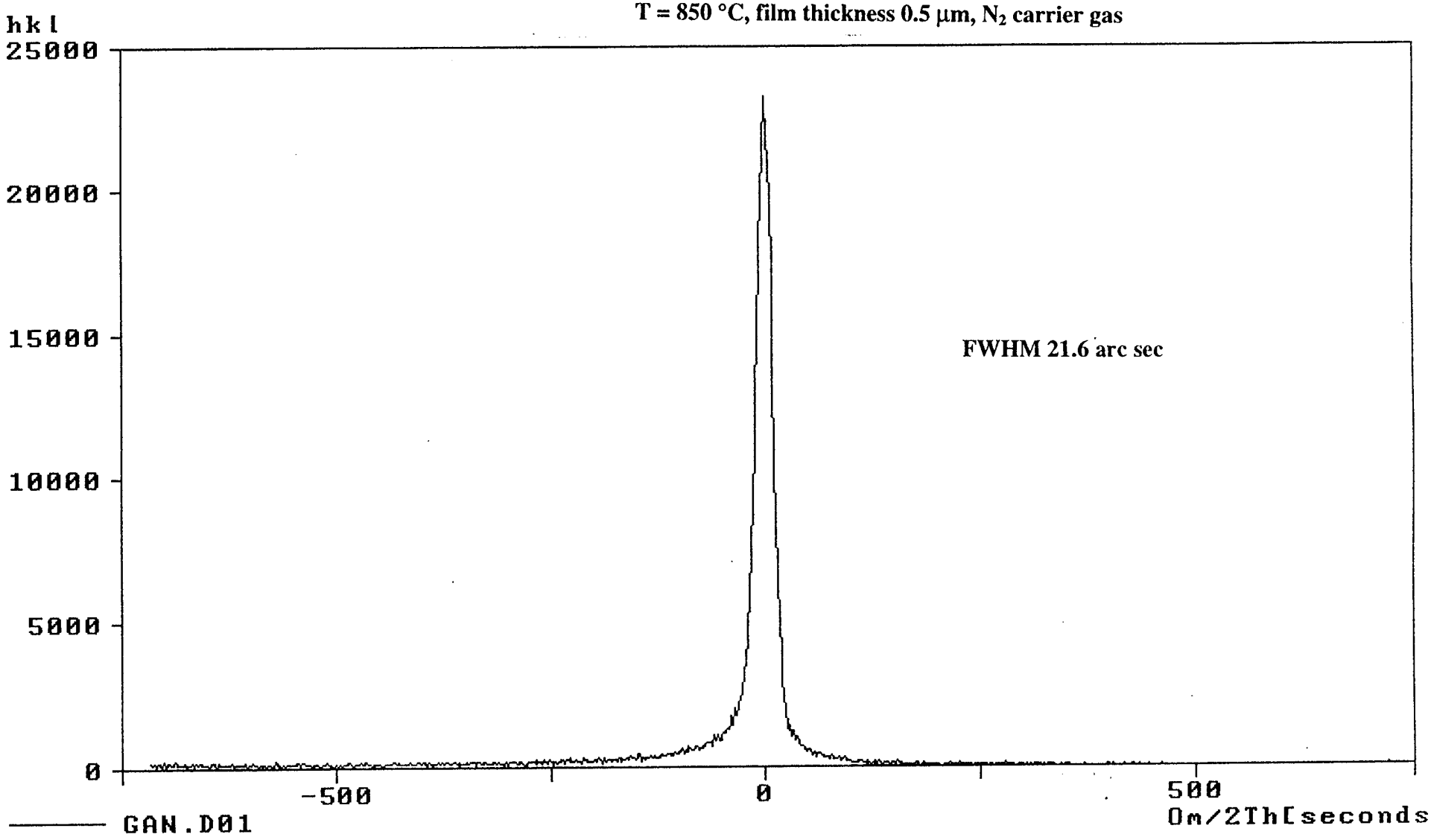

Fig. IV.4b. HRXR diffraction (double axis) GaN/$LiGaO_2$
omega scan
T = 850 °C, film thickness 0.5 μm, N_2 carrier gas

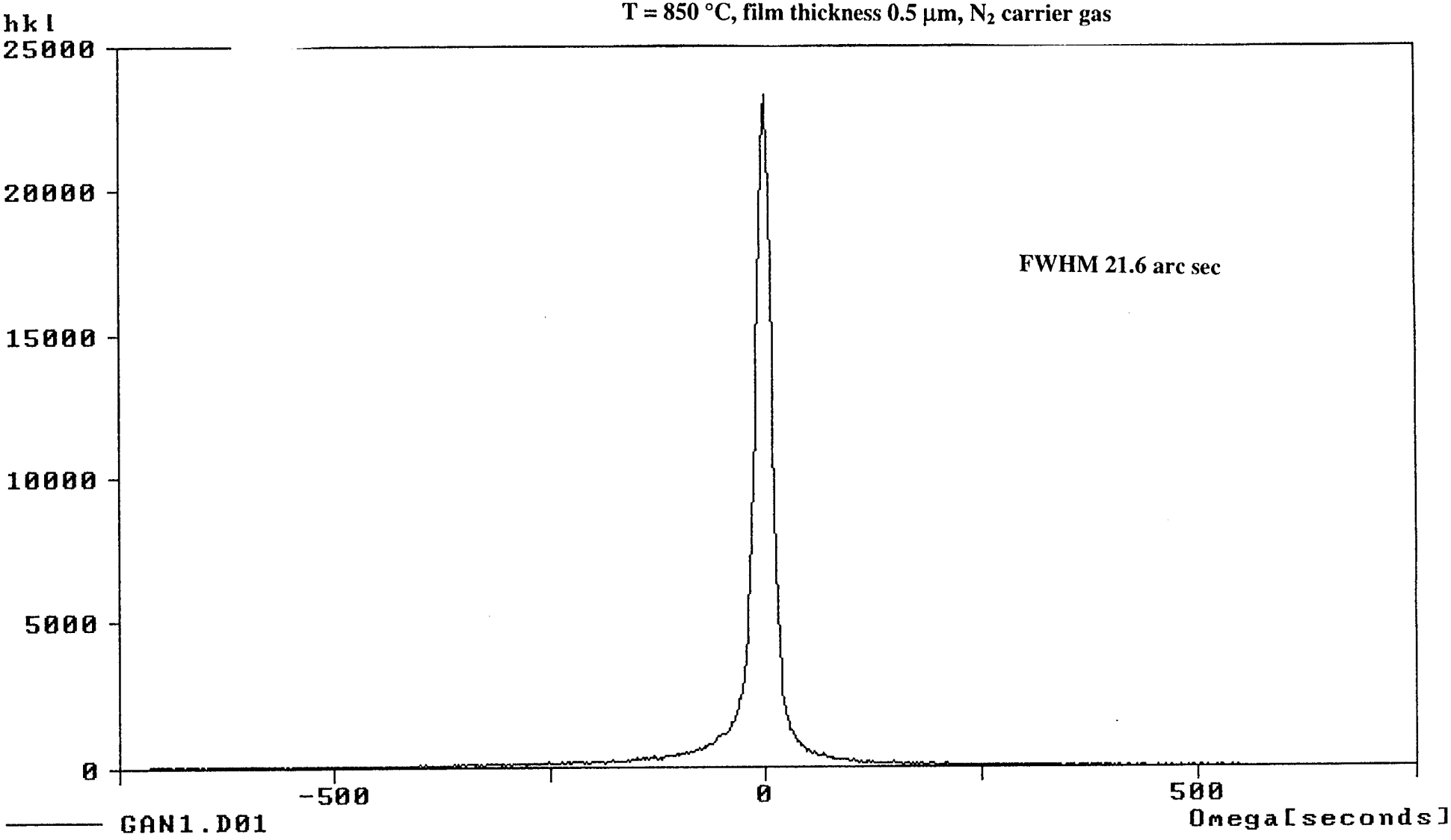

Fig. IV.4c. HRXR diffraction (triple axis) GaN/$LiGaO_2$
omega / 2θ scan
T = 850 °C, film thickness 0.5 μm, N_2 carrier gas

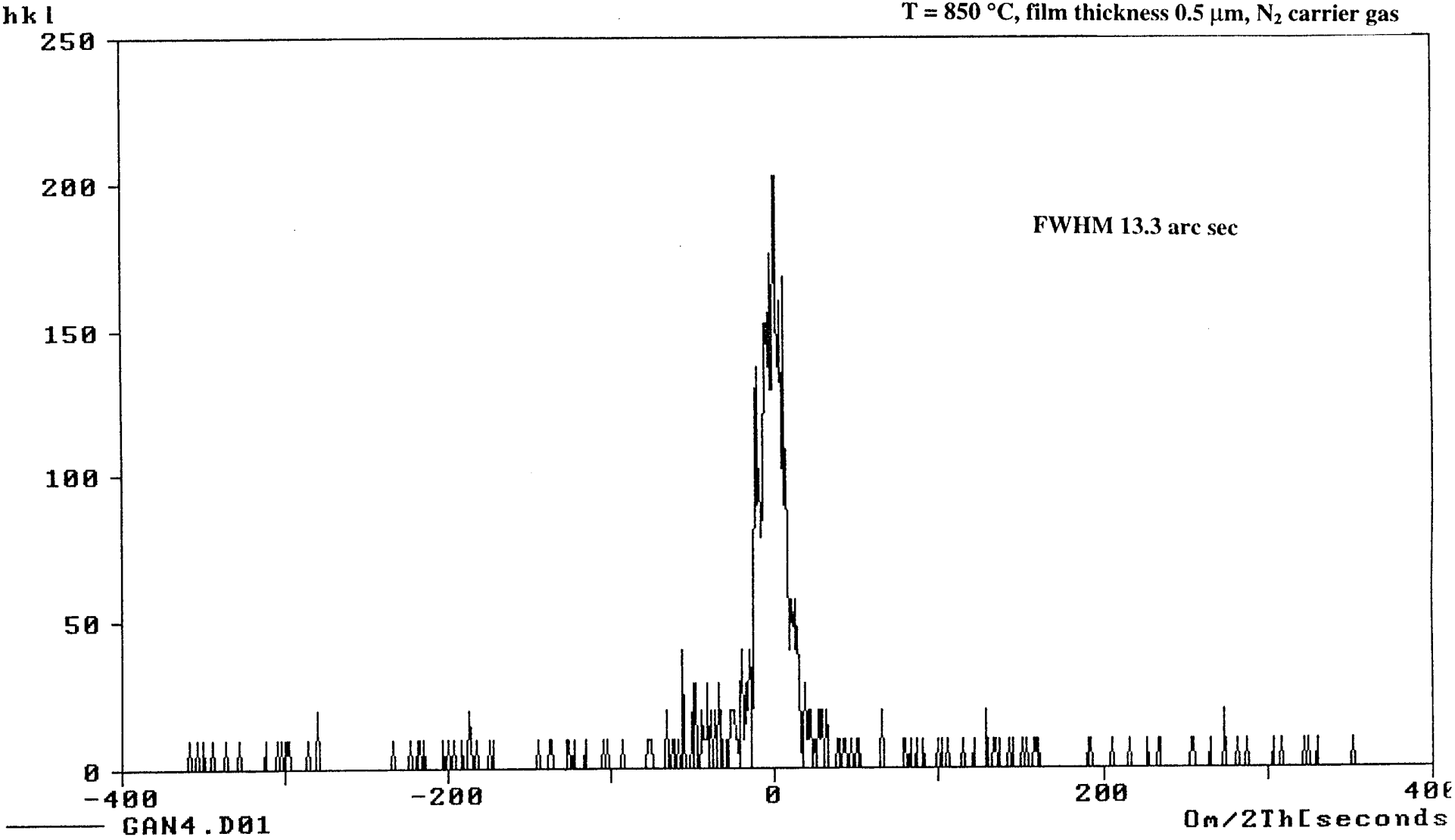

Fig. IV.4d. HRXR diffraction (triple axis) GaN/$LiGaO_2$
omega scan
T = 850 °C, film thickness 0.5 μm, N_2 carrier gas

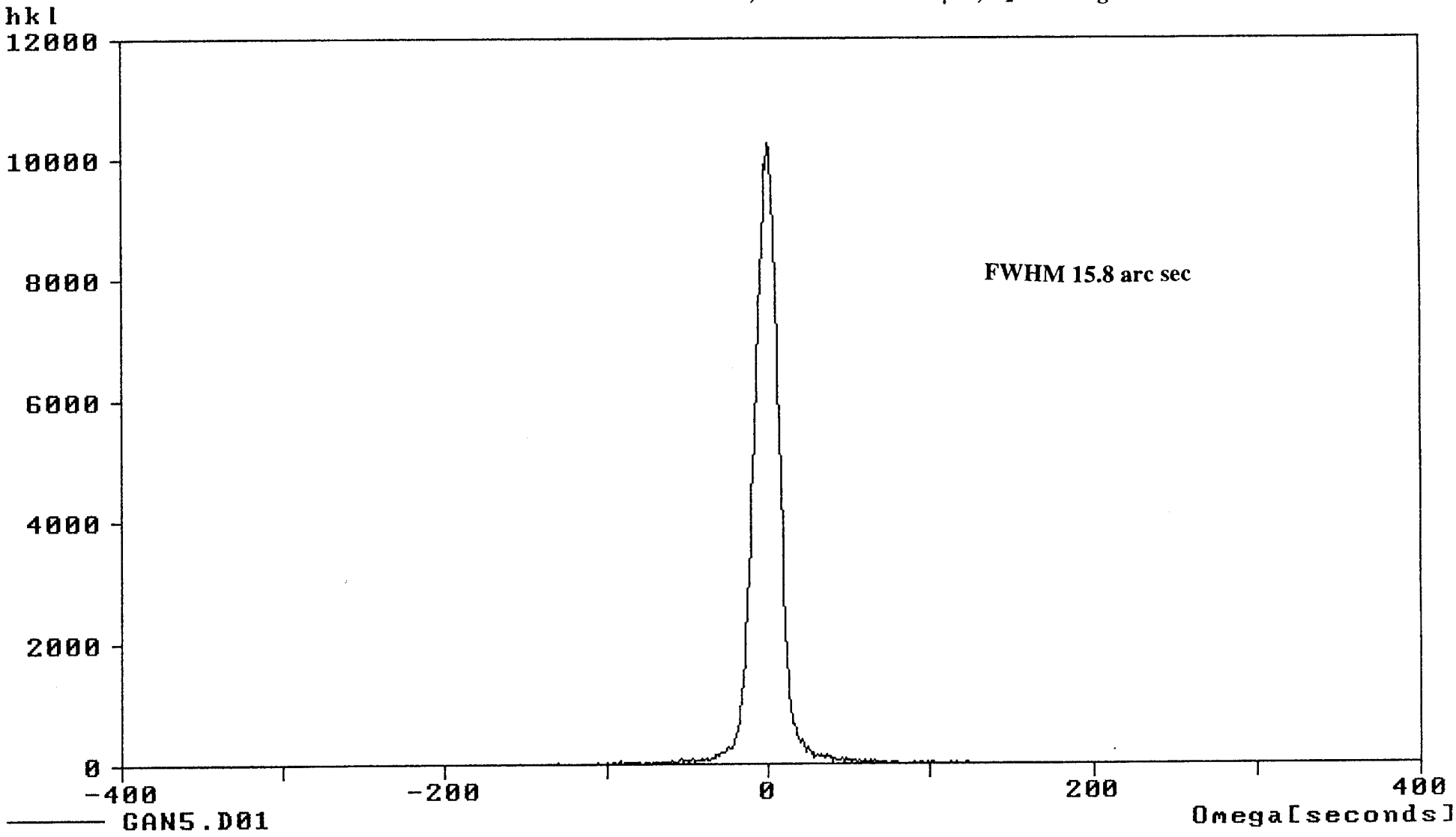

Table IV.2. X-ray FWHM values of GaN films on $LiGaO_2$ T = 850 °C, film thickness 0.50 μm

Scan	Double Axis (5-crystals)	Triple Axis (7-crystals)
Omega , arc sec	21.6	15.8
Omega / 2θ, arc sec	21.6	13.3

An AFM image of the GaN film on $LiGaO_2$ grown at 850 °C to a film thickness of 0.5 μm is shown in Fig. IV.5a-b. The surface is much more planar and much less faceted than in Fig. IV.2. The FWHM (double axis) values of GaN films grown on the three different substrates at T = 850 °C, using N_2 as a carrier gas, film thickness 0.5 μm are shown in Table IV.3.

Table IV.3. X-ray FWHM (double axis) values of GaN films on $LiGaO_2$, $LiAlO_2$ and α-Al_2O_3, T = 850 °C , film thickness 0.50 μm.

Substrate	(001)$LiGaO_2$	(110)$LiAlO_2$	(0112) r-Al_2O_3
Omega, arc sec	21.6	too wide	not taken
Omega / 2θ, arc sec	21.6	2632	39.5

The samples are still being characterized by SIMS, PL, and TEM. It appears, however, that very high structural quality GaN has been achieved by substitutions of N_2 for H_2. The influence of H_2 on the quality of the material is not clear at this time and could be related to either a substrate intereaction or surfactant effect. The poor results on $LiAlO_2$ are due to thermal decomposition of this substrate as determined in separate studies.

Fig. IV.6a-c show FTIR spectra from GaN which support the conclusion of high quality GaN grown on α-Al_2O_3 and $LiGaO_2$ substrates (compare the restrahlen peak structure with that for the GaN/$LiAlO_2$ structure). The estimated carrier concentrations (~9×10^{19} cm^{-3}) is high . All films grown using H_2 as a carrier gas exhibited poor quality as judges by FTIR.

The X-ray rocking curve of GaN layer grown on $LiGaO_2$ yielded the highest quality materials with a full width at half maximum value of 21.6 arc sec (double-axis) and 15.8 arc sec (triple axis) omega scans. Three sets of films have been grown in consecutive growth runs at (one at 800 °C and two at 850 °C). Similar results were obtained in each set. It appears that N_2 could play a key role in the growth of high quality GaN films.

During the next quarter, these films will be further characterized to verify the structural quality and assess the optical and electrical quality. A study of the initial stages of growth will be performed to better understand the difference in quality with a change

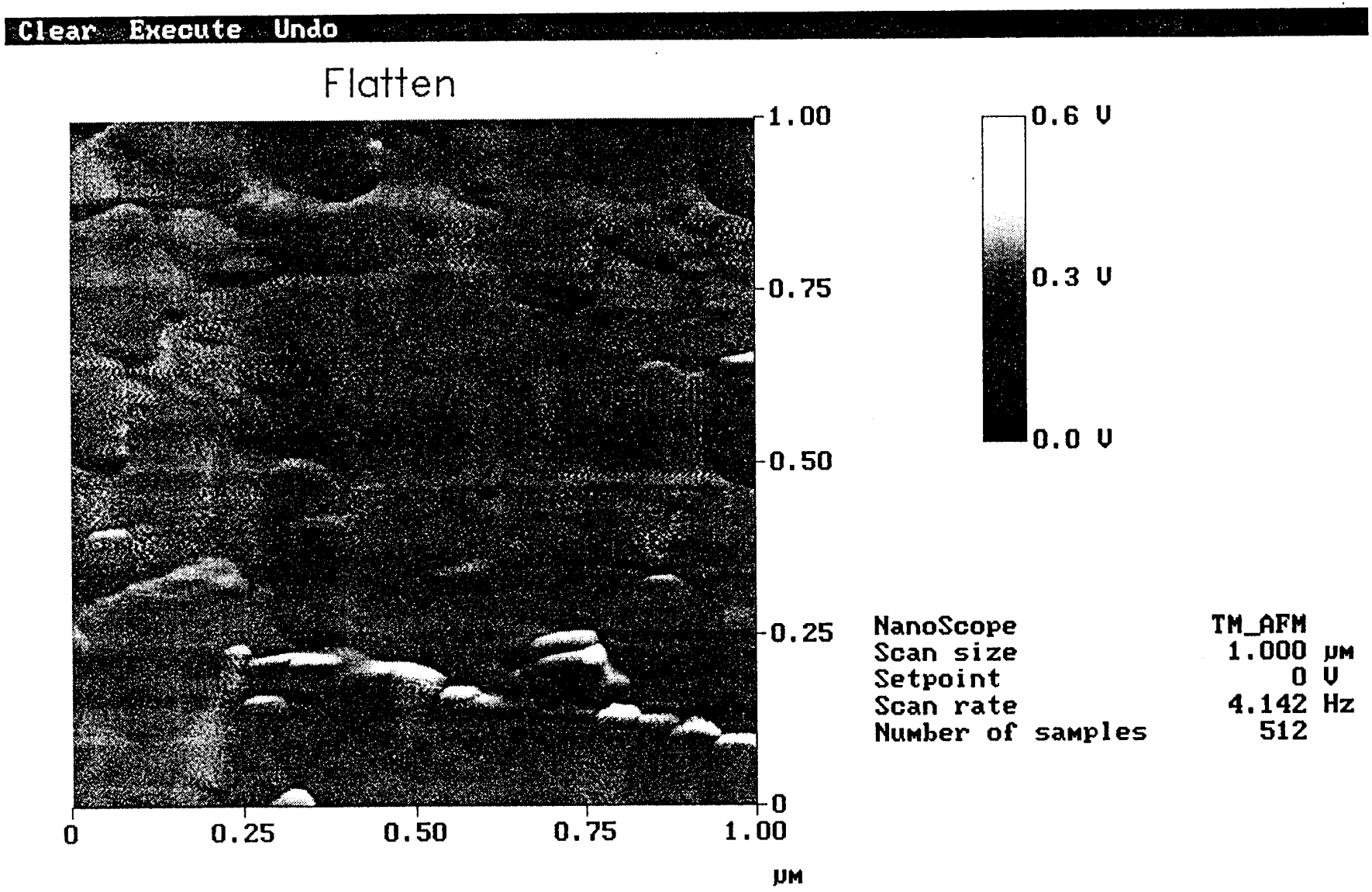

Fig. IV.5a. Atomic force microscopy image of GaN film on $LiGaO_2$ substrate, T = 850 °C, film thickness 0.5 µm, N_2 carrier gas

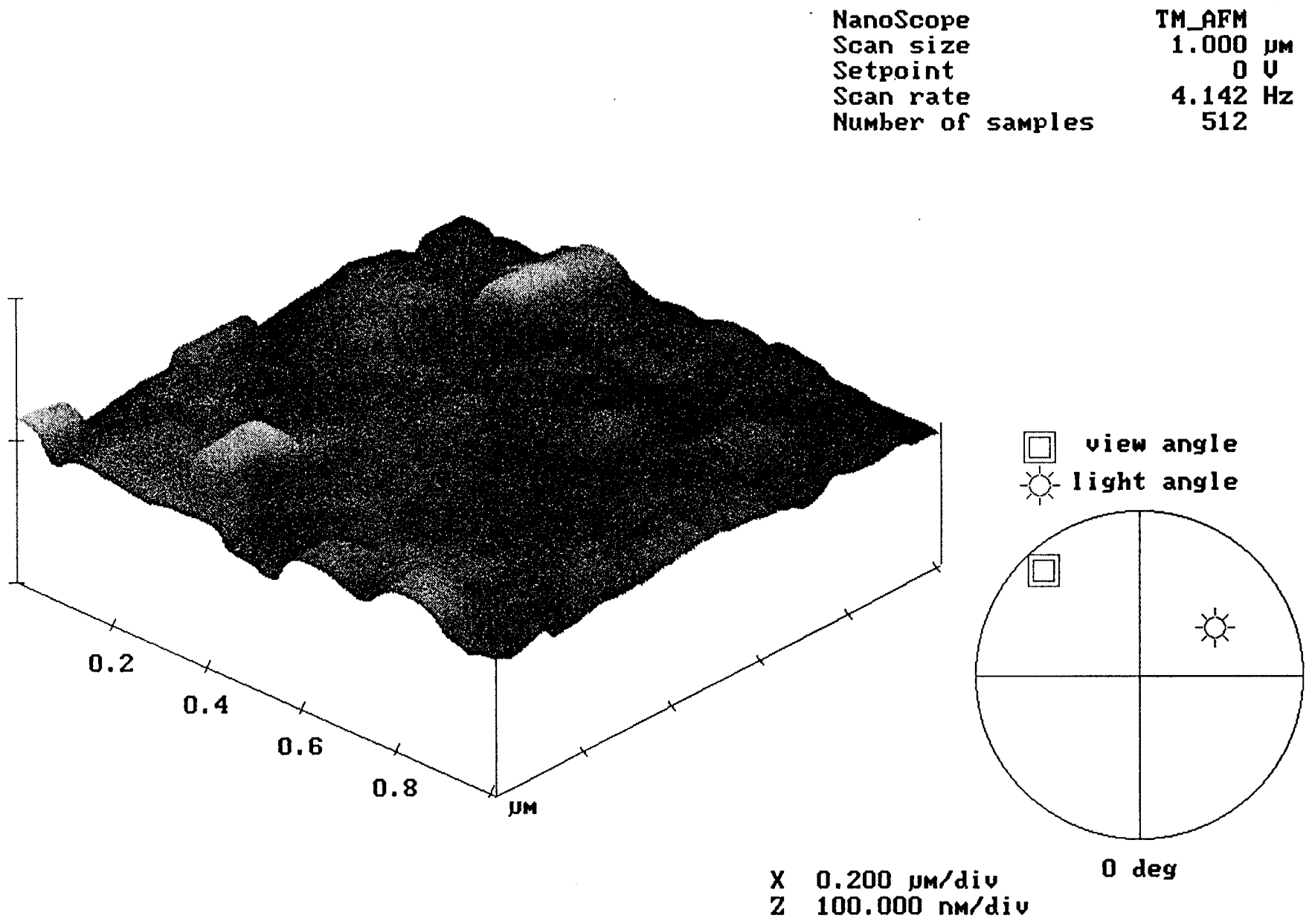

4a3in.012

Fig. IV.5b. 3-Dimentional view of the GaN film on $LiGaO_2$
T = 850 °C, film thickness 0.5 µm
N_2 carrier gas

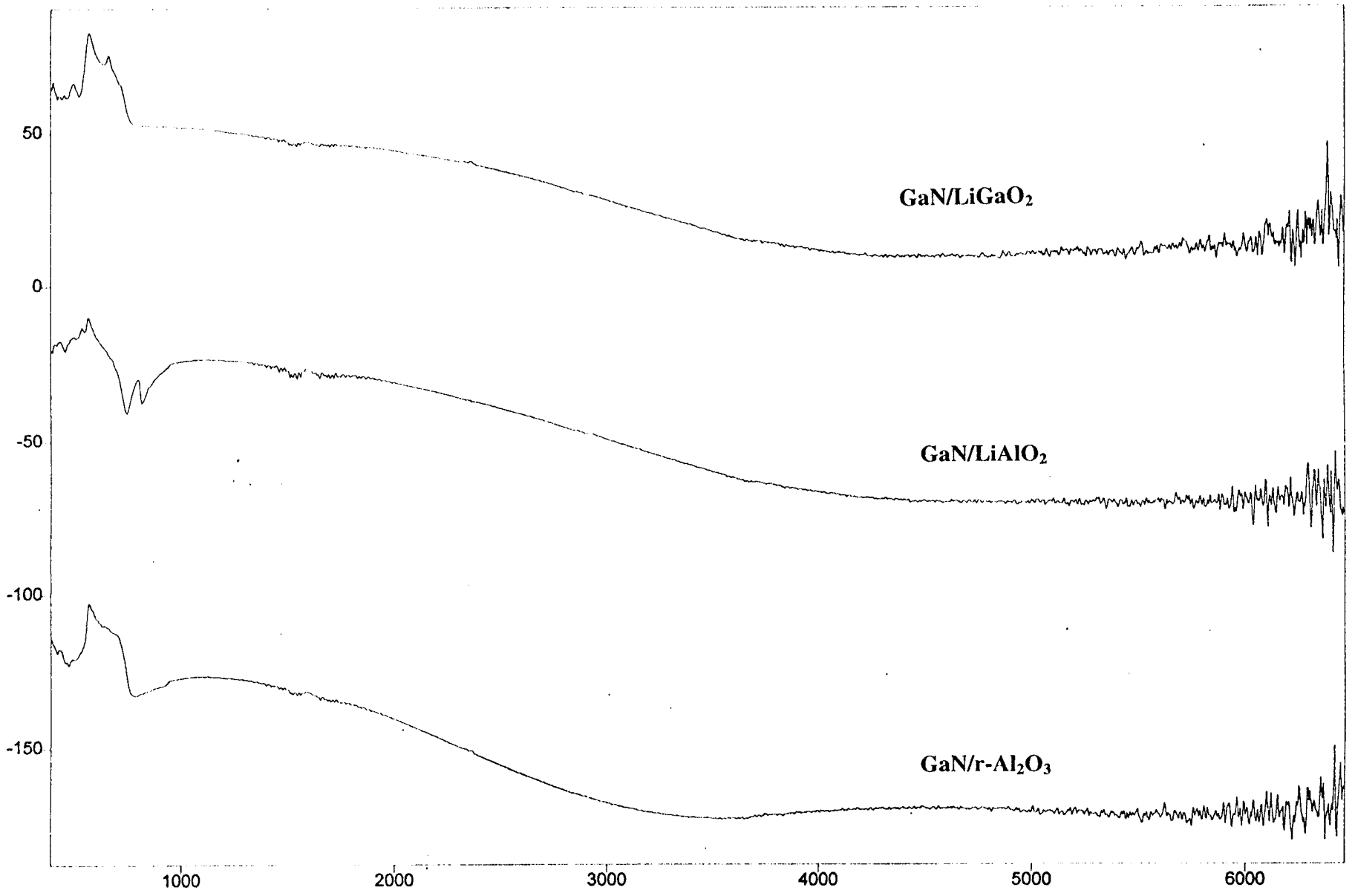

Transmittance / Wavenumber (cm-1)

Stacked X-Zoom CURSOR

File # 1 = GN12A

5/8/96 2:22 PM Res= 8

GaN-12A GaN/LGO 30deg, sm ap, unpol. SLOW;

Fig. IV.6a. GaN FTIR spectra of GaN films T = 850 °C, films thickness 0.5 μm N_2 carrier gas

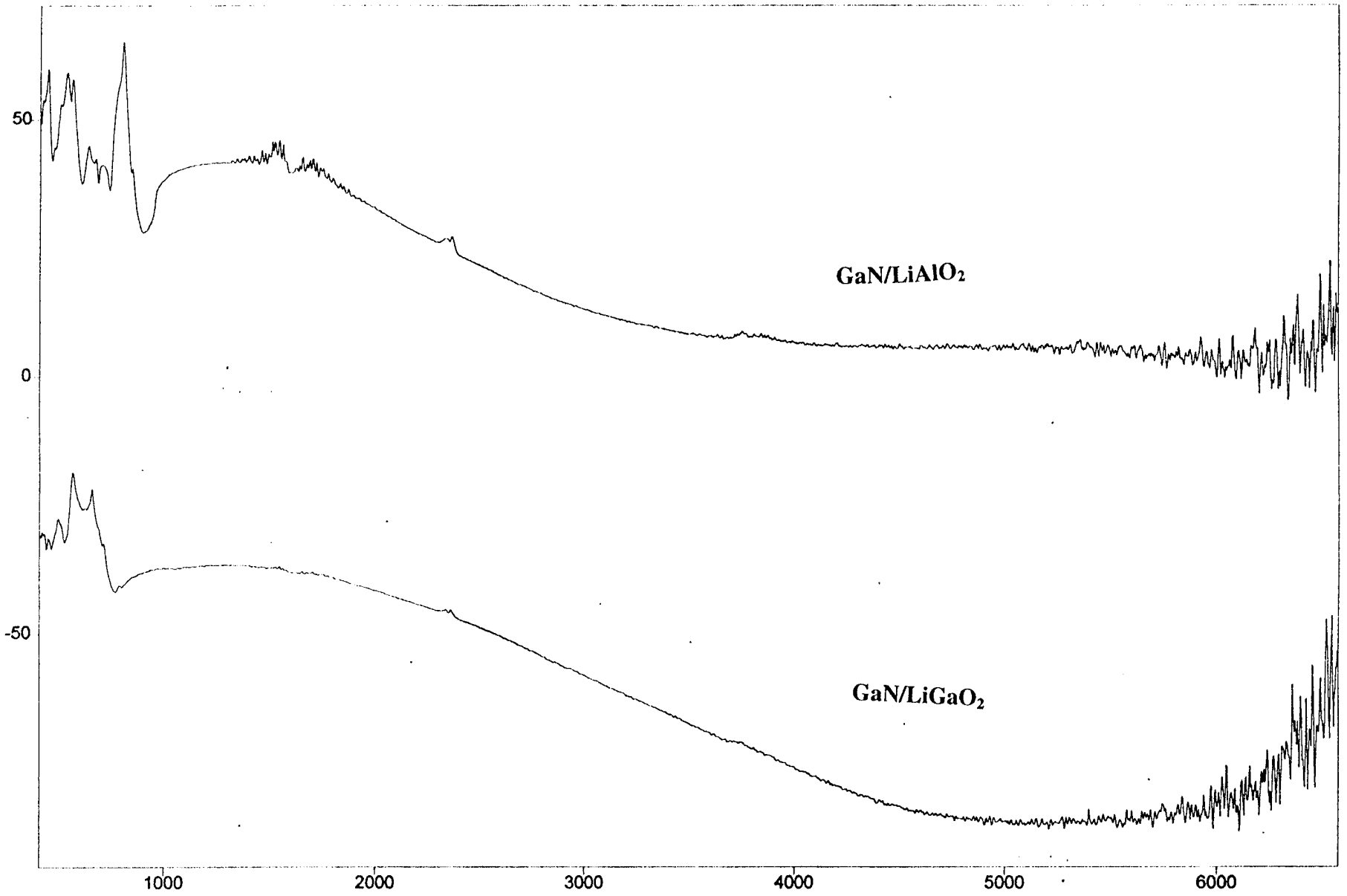

Transmittance / Wavenumber (cm-1)

Stacked X-Zoom CURSOR

File # 1 = GN4AB

5/9/96 12:51 PM Res= 8

GN-4 GaN/LAO 40deg, sm ap;

Fig. IV.6b. GaN FTIR spectra of GaN films T = 700 °C, films thickness 0.73 μm H_2 carrier gas

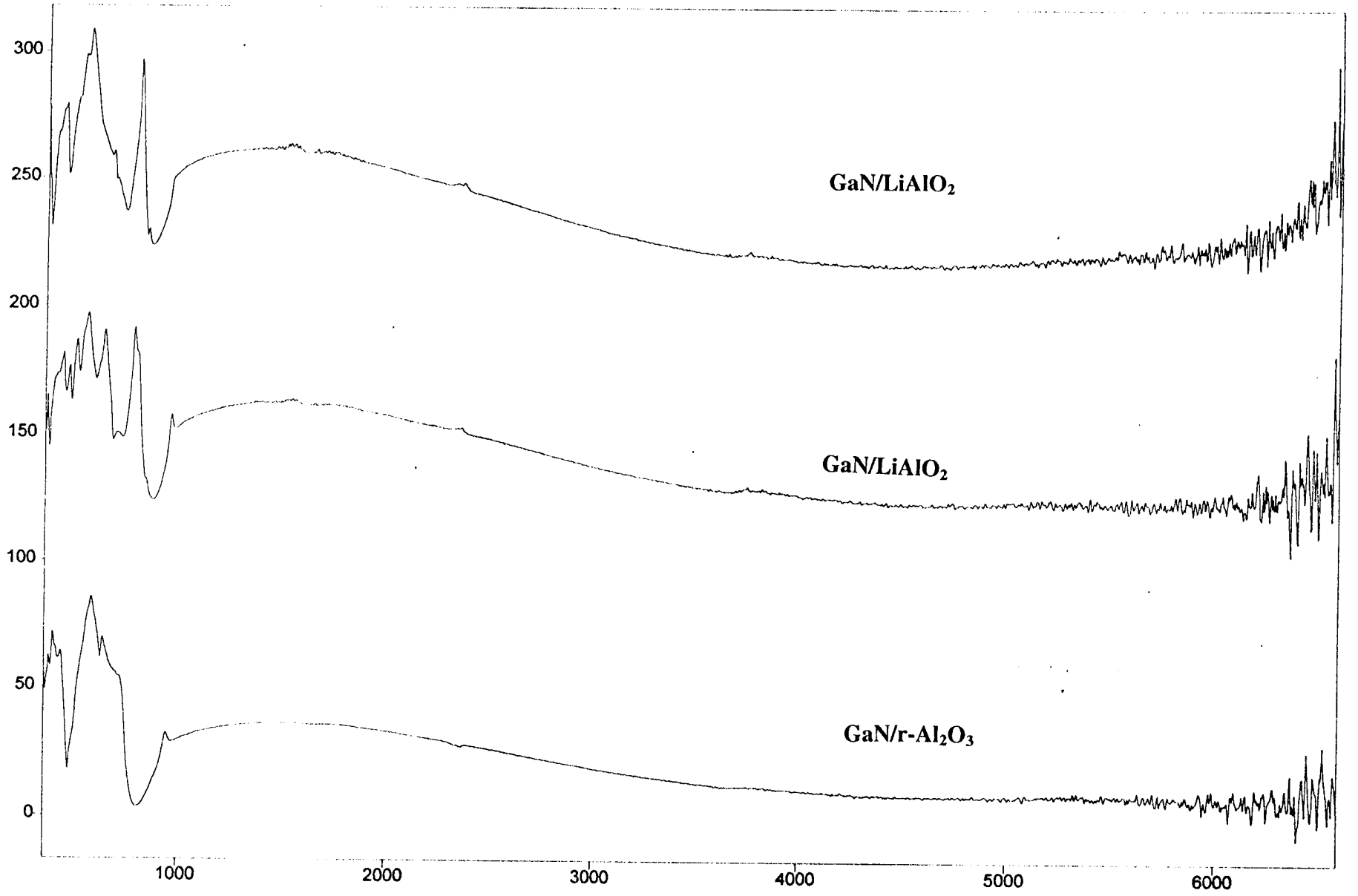

Transmittance / Wavenumber (cm-1)

File # 3 = GN6CA

GN-6 GaN/sapphire 40deg, sm ap;.

Stacked X-Zoom CURSOR

5/9/96 1:07 PM Res= 8

Fig. IV.6c. GaN FTIR spectra of GaN films T = 550 °C, films thickness 0.40 μm H_2 carrier gas

in carrier gas. We will than perform a parametric study to optimize the optical and electrical properties of the films.

(V) Diode Laser Materials (Peter Zory)

V.a. CdZnSe Quantum Well (QW) Diode Laser Material

Work is continuing on the lasing wavelength versus cavity length project. The goal is to determine if Coulomb Enhancement (CE) and Band Gap Renormalization (BGR), many-body effects predicted to be important for wide-bandgap semiconductor lasers, are in fact important for CdZnSe QW diode lasers. As mentioned previously, conventional QW laser theory correctly predicts the observed increase in lasing wavelength with cavity length but predicts a slope which is too small by a factor of 3. If BGR is included, the agreement is much worse with the slope actually changing sign. Preliminary results indicate that the addition of CE is in the right direction and that the correction may be sufficiently big to give good agreement with experiment. The quality of our experimental data has been improved recently using some new state-of-the-art, buried-ridge laser material provided by M. Haase of 3M. Our collaboration with Dr. P. Rees of Trinity College, Dublin, Ireland, is continuing.

V.b. InGaN QW LED Material

As reported previously, the liquid contact luminescence (LCL) technique we have been developing can be used to generate InGaN QW electroluminescence from DH (double heterostructure) p-GaN/InGaN/n-GaN MOCVD-grown material. While the spectra appear to be the same as obtained using electrical contacts, the efficiency of light emission for a given current density appears to be considerably lower for samples with very thin p-GaN layers. The reason may have to do with carrier leakage in the LCL case because of the higher drive voltages required to obtain the same current density. An understanding of this phenomenon may have some bearing on the contact resistance problem present in conventional metal contact devices.

Since the DH material described above is grown on an insulating sapphire substrate, it is necessary to remove the p-GaN and InGaN layers on part of the wafer in order to make contact to the n-GaN layer. We have discovered that we can do this using the pulsed electrochemical setup shown in Fig. V.1. Using an electrolyte composed of 40 parts ethylene glycol, 20 parts water and 1 part 85% phosphoric acid, an etch rate of about 1.5 μm/hr. was achieved with R_{var} = 2K ohms and 220 volt, 300 microsecond-wide pulses at a repetition rate of 100 Hz. Fig. V.2a shows the behavior of the current pulse at $t = 0$ and $t > 0$, and Fig. V.2b shows the behavior of the trailing edge current as the etch front moves through the material. When the etch front approaches the QW (p-n junction), there is a sharp drop in the trailing edge current. Depending on drive conditions and material quality, the trailing edge current oscillates to varying degrees while the etch front moves through the n-type material.

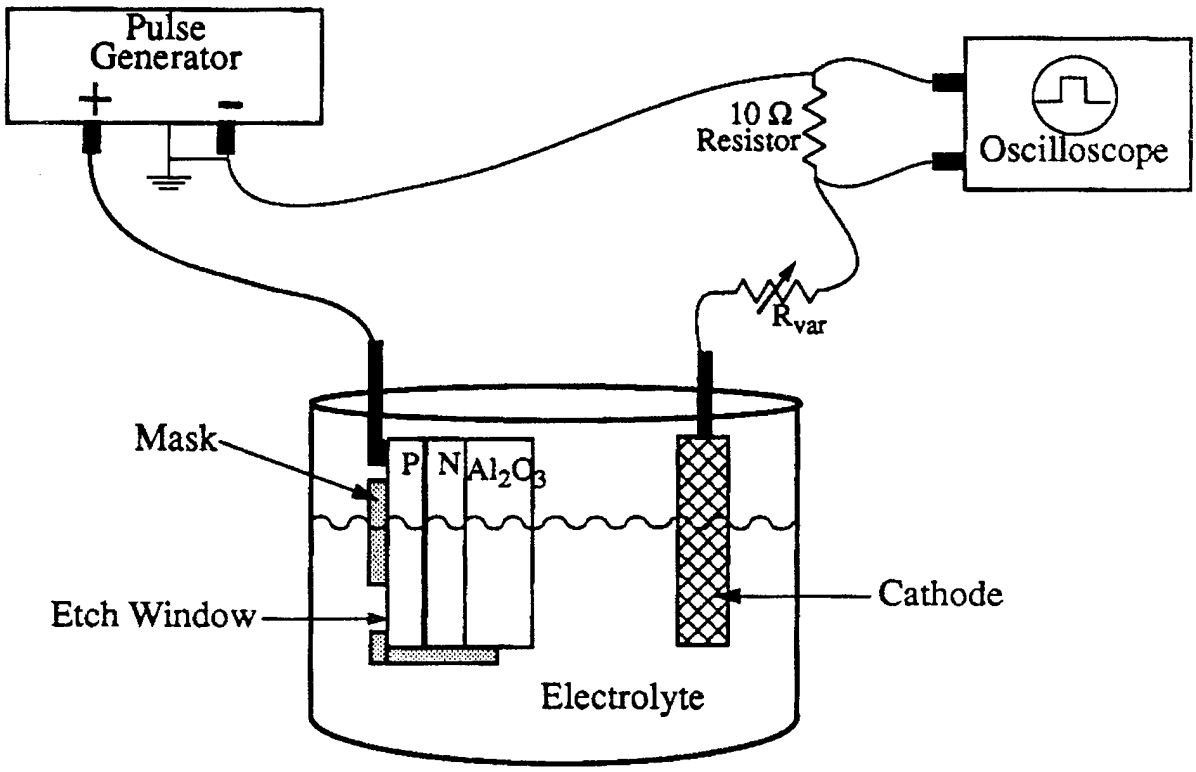

(a) Etching set-up

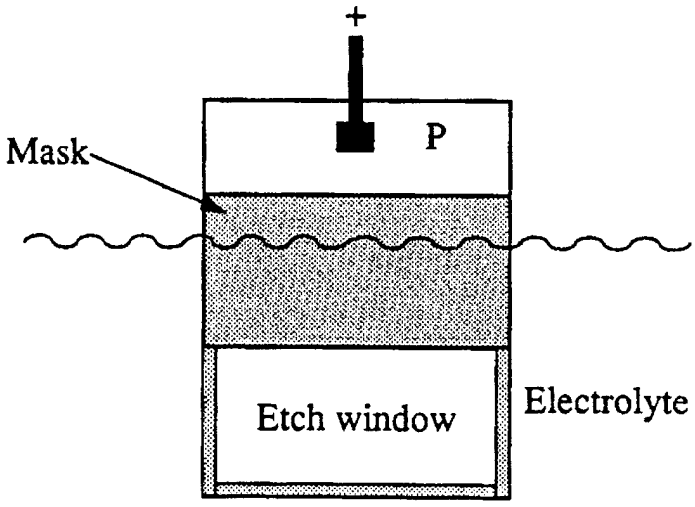

(b) Front view of a sample

Fig. V.1. Electrochemical etching set-up

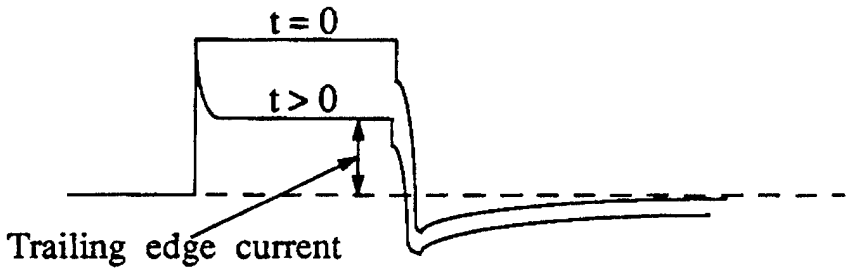

(a) Typical pulse shape

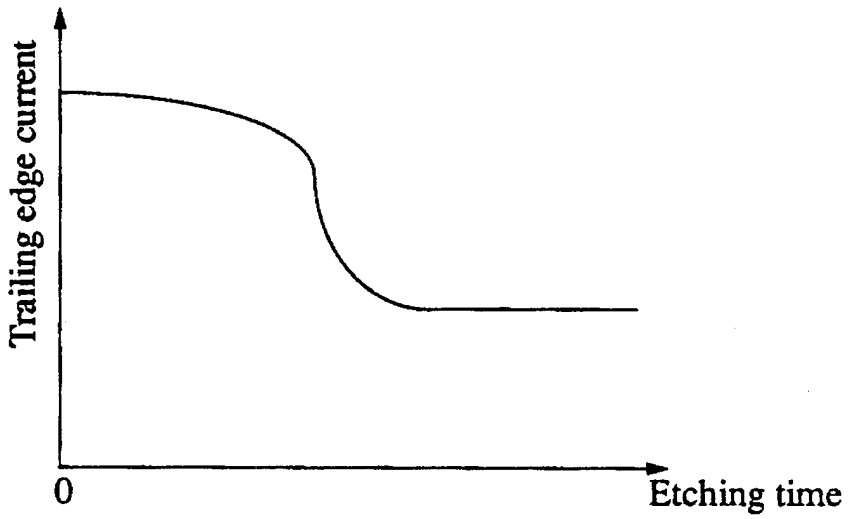

(b) Typical trailing edge current change

Fig. 2 Typical current change during the etching

(VI) Theoretical Calculations of Dopants of ZnSe (G.F. Neumark)

As reported previously, we have been able to set up appropriate equations for the average carrier concentration in the case of potential fluctuations in a semiconductor (where such fluctuations are present in heavily doped ZnSe:N). However, these equations contain the Fermi level and the screening length as parameters, and the system of equations must be solved self-consistently. As a result, obtaining solutions is obviously a non-trivial problem. We have noted that V.N. Bondarev, P.P. Pikhitsa, (Phys. Lett. **A196**, (1994), 247) have elegantly solved a somewhat similar problem, namely that of fluctuations in ionic conductors. We are therefore presently trying to set up a collaborative effort with them, under an exchange program. In the meantime, we have deferred work on these equations.

We have also continued our investigation [Prog. Report of Sept.-Nov. 1995] regarding the likelihood of non-equilibrium dopant incorporation during low-temperature growth, such as MBE. We have concluded that at low growth temperatures, bulk growth is likely to be "quasi"-equilibrium, but that dopant incorporation is often non-equilibrium. We have carried out a careful analysis of literature results, which corroborates our conclusion. A particular example, for ZnSe:N, is work by Qiu et. al. (Appl. Phys. Lett., **59**, (1991), 2992), which shows that net acceptor concentrations increase with decreasing growth temperature. The cause of this difference in behavior is likely to be due, at least in part, to the (orders-of-magnitude) difference in the magnitudes of the arriving atomic fluxes. It can be noted that this conclusion is in agreement with the hypothesis of one of us [Neumark, Phys. Rev. Lett. **62**, 1800 (1989)] that good doping in wide-gap materials often requires non-equilibrium dopant incorporation.

(VII) Wide Band-gap Semiconductors for Short Wavelength Emitters (J.I. Pankove)

Our report for this quarter focuses on the continuation of our doping studies, emphasizing Mg-doping which can simultaneously render GaN films p-type and introduce short wavelength recombination centers. Temperature dependent photoluminescence spectroscopy was used to explore the defect levels introduced upon doping with magnesium.

To explore the role of activation of the Mg acceptors, three sets of data were collected for a lightly Mg-doped sample with $p = 7 \times 10^{16}$ cm^{-3} and $\mu = 15$ cm^2/Vs. The first measurement examined the temperature dependence of the PL spectrum for the fully-activated p-type sample. Next, the sample was annealed in flowing forming gas at 600°C for one hour and again at 700°C for two hours in an attempt to de-activate some of the shallow acceptor centers. A slight increase in resistivity was detected after the anneal. After recording the temperature dependent PL spectra for the annealed sample, the sample was then treated with low-energy electron beam irradiation (LEEBI) at 15 kV to re-activate the shallow acceptors. The LEEBI treatment was found to increase the PL signal by more than an order of magnitude.

Normalized temperature dependent photoluminescence spectra of the annealed and re-activated Mg-doped samples are shown in Fig. VII.1. A comparison of the low

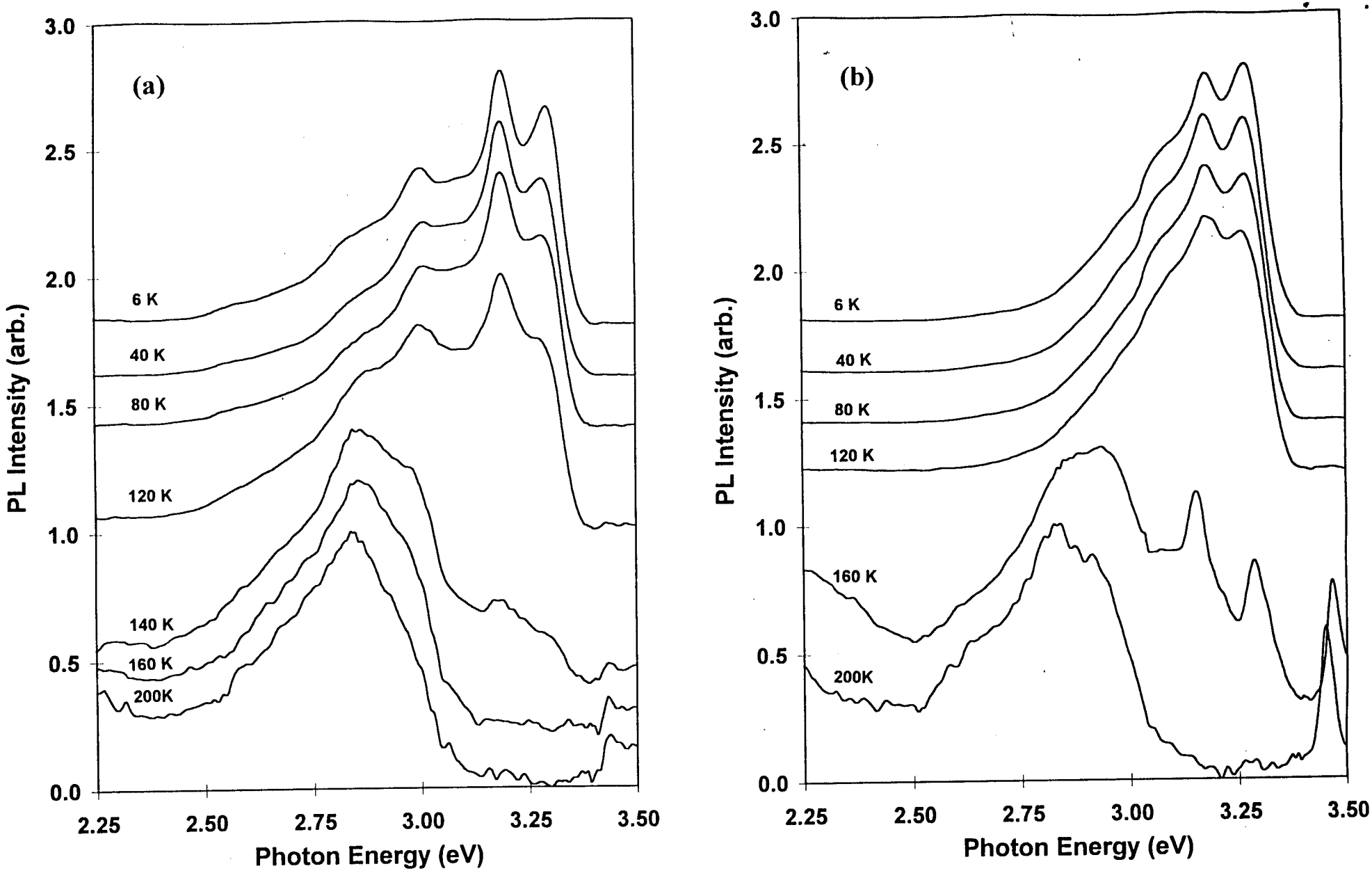

Fig. VII.1. Normalized photoluminescence spectra of GaN:Mg at several temperatures (a) after annealing in forming gas, and (b) after annealing and subsequent LEEBI treatment.

temperature spectra revealed that the ratio between the highest energy (3.28 eV) peak and the second peak (3.19 eV) was not the same in the two samples. In fact, in both cases this ratio decreased as the temperature was raised. This effect is inconsistent with the model which describes the second peak as a phonon replica of the 3.28 eV peak. The linear configurational coordinate model of electron-phonon interaction[1] predicts that for interactions involving high energy phonons ($h\omega_\omega$ = 91 meV), the relative intensities of phonon replicas will remain constant as the temperature is changed. This result indicates that these two peaks have different activation energies for thermal quenching and suggests that the peak at 3.19 eV is an independent defect level.

When a group II element is incorporated into GaN it can take one of two substitutional lattice sites. Magnesium occupying a gallium site (Mg_{Ga}) is expected to act as a single acceptor level and contribute one luminescence peak. Magnesium on a nitrogen site (Mg_N), however, may be capable of capturing up to three electrons and could thus contribute three acceptor levels and, correspondingly, three luminescence peaks. Four luminescence peaks have been observed in GaN:Zn and have been attributed to zinc occupying both substitutional sites.[2] Three distinct luminescence peaks have been reported in association with magnesium in GaN. Room temperature photoluminescence and electroluminescence has been observed at ~2.8 eV,[3,4] ~ 2.95 eV,[3,5] and ~ 3.28 eV.[3,6] With the addition of the level at 3.19 eV, a total of four levels are observed and may be explained by assuming that the magnesium takes both substitutional sites, Mg_{Ga} and Mg_N. We cannot at this time, however, discount the possibility of the involvement of other mechanisms such as magnesium complexes with hydrogen in one or more of these levels.

(VIII) Theoretical Models for Blue/Green Semiconductor Laser Structures (Reinhart Engelmann)

The problem of non-radiative and/or non-lasing radiative transitions in the GaN laser system is addressed. It is emphasized that a systematical experimental analysis of the current components in GaN based pn junctions is still lacking and should be performed in order to elucidate and, eventually, minimize the non-radiative and/or non-lasing radiative components in the current components in GaN based single and multiple QW p-n junctions.

The various current components in GaAs p-n junctions have been extensively studied in the sixties which eventually has led to dramatic improvements of the internal quantum efficiency of GaAs LEDs approaching 100%, providing an important basis for low threshold-current diode lasers. GaN based LEDs are, in a way, strange newcomers with unexpectedly high external efficiencies, but their internal quantum efficiencies are still only about 20%.[7] In addition, the radiative transitions utilized in these structures are transitions between donor and acceptor centers with the acceptors being optically very deep. These transitions saturate at high injection and do not lase.[8] Thus, to demonstrate lasing in these new diode systems has proven to be a difficult task, and in fact has been achieved only very recently.[9-11]

For lasing it is necessary to enhance the radiative recombination path from conduction to valence band on a relative basis by reducing the competing non-lasing paths. A further complication in achieving low-threshold lasing is the possibility that p-type conduction in the cladding layer occurs in a deep impurity band which would make hole injection into the active lasing region more difficult. Preliminary analysis of such lasers[12,13] indicate a substantial current component not involved in lasing transitions. For these reasons a systematic experimental analysis of current components in GaN based p-n junctions is required. The analysis should include semi-log current-voltage and spectrally resolved light output-vs. voltage characteristics for various temperatures. Such characteristics provide valuable information, such as ideality factor, activation energy, radiative vs. non-radiative transitions, required to estimate the relative strengths of various current components and to identify their potential origin.

Current components to be considered are:

A) Recombination currents in the active QW layers due to
   1) band-to-band transitions (desired for lasing).
   2) impurity transions
   3) tunneling transitions
   4) Shockley-Read type transitions via defect traps
   5) surface recombination resulting from defect transitions at the QW-barrier interfaces and/or the semiconductor surface

B) Recombination currents resulting from injection into barrier or cladding layers comprising similar transitions as listed under A).

The high defect density reported in the nitride materials[14] is expected to provide substantial contributions from mechanisms 4) and 5). For space-charge region recombination, these transitions should lead to a large ideality factor near n=2 which would make them dominant only at low injection. But the high doping density in the cladding layers, particularly for thin single QW structures, could generate a component 3) which can be identified from a characteristic temperature dependence for the ideality factor (temperature independence of the semi-log slope) at the proper bias levels, and, in case of injection into barrier or cladding layers, by a characteristic shift of the emission peak with applied voltage. It appears that most impurity transitions in the nitrides are radiative and could be identified by corresponding bands in the emission spectrum that would tend to saturate at higher injection. Injection into barriers or cladding layers would also produce emission peaks that are characteristic for their impurity transition, expected to be particularly pronounced for the p-type cladding layer with its deep acceptor levels. The determination of the activation energies of the current components can provide further aid in identifying the underlying transitions.

For meaningful analysis a careful evaluation of, and correction for, the diode series resistance is required. Current experimental structures exhibit high values, ranging of 12 to 36 Ω depending on contact stripe size [3-5]. Also, a certain degree of non-ohmic behavior of the contact resistance cannot be ruled out which complicates such an analysis. A study of band-to-band emission intensity vs. voltage can provide the required series

resistance correction based on the expected ideality factor of nearly n =1 for such a relationship. Control measurements with equivalent homojunction structures could aid in the current component analysis.

In summary, it is suggested to launch a comprehensive investigation of current components in single and multiple QW laser structures aiming at understanding the non-lasing recombination paths and minimizing their contribution.

References:

[1] B. Monemar and L.Samuelson, Phys. Rev. **B 18** (2), 809 (1978).

[2] B. Monemar, O. Lagerstedt, and H.P. Gislason, J. Appl. Phys. **51** (1), 625 (1980).

[3] H. Amano, M. Kitoh, K. Hiramatsu, and I. Akasaki, J. Electrochem. Soc. **137** (5), 1639 (1990).

[4] H. Amano, M. Kitoh, K. Hiramatsu, and I. Akasaki, Inst. Phys. Conf. Ser. No. 106, 725 (1990).

[5] H.P. Maruska, D.A. Stevenson, and J.I. Pankove, Appl. Phys. Lett **22** (6), 303 (1973).

[6] M.S. Brandt, N.M. Johnson, R.J. Monlar, R. Singh, and T.D. Moustakas, Appl. Phys. Lett. **64** (7), 2264 (1994).[7] George Craford, private communication.

[7] George Craford, private communication.

[8] S. Nakamura, M. Senoh, N. Iwasa, S. Nagahama, T. Yamada, and T. Mukai, "Superbright green InGaN single-quantum-well-structure light-emitting diodes," Jpn. J. Appl. Phys. 34, Part 2 (10B), pp. L1332-L1335 (15 October 1995).

[9] S. Nakamura, M. Senoh, S. Nagahama, N. Iwasa, T. Yamada, T. Matsushita, H. Kiyoku, and Y. Sugimoto, "InGaN-based multi-quantum-well-structure laser diodes," Jpn. J. Appl. Phys. 35, Part 2 (10B), pp. L74-L76 (15 January 1996).

[10] S. Nakamura, M. Senoh, S. Nagahama, N. Iwasa, T. Yamada, T. Matsushita, H. Kiyoku, and Y. Sugimoto, "InGaN multi-quantum-well structure laser diodes grown on $MgAl_2O_4$ substrates," Appl. Phys. Lett. 68 (15), pp.2105-2107 (8 April 1996).

[11] S. Nakamura, M. Senoh, S. Nagahama, N. Iwasa, T. Yamada, T. Matsushita, H. Kiyoku, and Y. Sugimoto, "Characteristics of InGaN multi-quantum-well-structure laser diodes," Appl. Phys. Lett. 68 (23), pp.3269-3271 (3 June 1996).

[12] P.G. Elisev, V.A. Smagley, and M. Osinski, "Analysis of impurity-related blue emission in Zn-doped GaN/InGaN/AlGaN double heterostructure," OE/LASE'96 Conference 2693: Physics and Simulation of Optoelectronic Devices IV, San Jose, CA, 29 Jan - 2 Feb 1996.

[13] M. Osinski and P.G. Eliseev, "Optimization of active-layer and cavity design parameters for low threshold GaN/AlGaN double-heterostructure diode lasers," OE/LASE'96 Conference 2693: Physics and Simulation of

Optoelectronic Devices IV, San Jose, CA, 29 Jan - 2 Feb 1996.

[14] S.D. Lester, F.A. Ponce, M.G. Craford, and D.A. Steigerwald, "High dislocation densities in high efficiency GaN-based light-emitting diodes," Appl. Phys. Lett. 66 (10), pp.1249-1251 (6 March 1995).

Publications:

- "*Ex Situ* Formation of HgSe Electrical Contacts to ZnSe", J.J. Fijol, J.T. Trexler, L. Calhoun, R.M. Park and P.H. Holloway, J. Vac. Sci. Technol. **B14**, 159 (1996).
- "Compensation in heavily N-doped ZnSe: a luminescence study," C. Kothandaraman, G.F. Neumark, and R.M. Park, J. Crystal Growth, **159**, (1996), 298-301.
- "Time-resolved luminescence studies of heavily Nitrogen doped ZnSe," C. Kothandaraman, I. Kuskovsky, G.F. Neumark, and R.M. Park, App. Phys. Lett., submitted.
- "Emergence of deep levels in n-type ZnSe under hydrostatic pressure," T.M. Ritter, B.A. Weinstein, R.M. Park and M.C. Tamargo, Phys. Rev. Lett., **76**, 964 (1996).
- "High Pressure Photoluminescence of deep levels in n-type ZnSe: Emergence of deep states in the gap," T.M. Ritter, B. Iota, B.A. Weinstein, M. Tamargo and R.M. Park, APS Bulletin, **41**, 671 (1996).
- "Exciton recombination dynamics in ZnCdSe/ZnSe quantum wells," R.A. Taylor, R.A. Adams, J.F. Ryan and R.M. park. Crystal Growth, **159**, 822 (1996)
- "Impact of surface stoichiometry control during the initial stages of growth on the stacking fault concentration in ZnSe epilayers grown by MBE," M.H. Jeon, L.C. Calhoun, B.P. Gila, M.H. Ludwig and R.M. Park, submitted to APL.
- "Ion implanted GaN FET," J.C. Zolper, R.J. Shul, A.G. Baca, R.G. Wilson, S.J. Pearton and R.A. Stall, Appl. Phys. Lett. **68** 2273 (1996).
- "Ca and O ion implantation doping of GaN," J.C. Zolper, R.G. Wilson, S.J. Pearton and R.A. Stall, Appl. Phys. Lett. **68** 1945 (1996).
- "Wet and dry etching of $LiGaO_2$ and $LiAlO_2$," J.W. Lee, S.J. Pearton, C.R. Abernathy and B.L. Chai, J. Electrochem. Soc. (August issue, 1996).
- "The Incorporation of H into III-V Nitrides During Processing," S.J. Pearton, R.J. Shul, R.G. Wilson, F. Ren, J.M. Zavada, C.R. Abernathy, C.B. Vartuli, J.W. Lee, J.R. Mileham and J.D. Mackenzie, J. Electron. Mater. **25** 84 (1996).
- "Electrical Transport in p-GaN, n-InN and n-InGaN," W. Geerts, J.D. Mackenzie, C.R. Abernathy, S.J. Pearton and T. Schmieder, Solid state electron. (in press).

Presentations:

- "Effects of Hydrogen on Ca and Mg Acceptors in GaN," J.W. Lee, S.J. Pearton, J.C. Zolper and R.A. Stall, 186th ECS meeting, Los Angeles May 1996.
- "Plasma Etching of the III-V Nitrides," R.J. Shul, S.J. Pearton and C.R. Abernathy, 186th ECS Meeting, Los Angeles May 1996-Invited.
- "III-Nitride Ion implantation and Device Processing," J.C. Zolper, R.J. Shul, A.G. Baca, S.J. Pearton, C.R. Abernathy, R.G. Wilson, R.A. Stall and M. Shur, 186th ECS Meeting, Los Angeles, CA May 1996-INVITED.
- "Ohmic Contacts on Binary and Ternary III-Nitrides," F. Ren, S.J. Pearton, S.M. Donovan, C.R. Abernathy and M.W. Cole, 186th ECS Meeting Los Angeles, May 1996-INVITED.
- "Properties of H, and C in GaN, S.J. Pearton, C.R. Abernathy, J.W. Lee, C.B. Vartuli, J.D. Mackenzie, F. Ren, R.G. Wilson, J.M. Zavada, R.J. Shul and J.C. Zolper, MRS Spring Meeting, SF, April 1996.
- "Plasma Chemistries for dry etching GaN, InGaN and InAlN," S.J. Pearton, R.J. Shul, G.F. McLane and F. Ren, MRS Spring Meeting, SF, April 1996.
- "Dry Etch Damage in InN, InGaN and InAlN," S.J. Pearton, J.W. Lee, J.D. Mackenzie, C.B. Vartuli, S.M. Donovan, C.R. Abernathy, R.J. Shul, F. Ren and J.R. Lothian, MRS Spring Meeting, SF, April 1996.
- "High Temperature Surface Degradation of III-V Nitrides," C.B. Vartuli, S.J. Pearton, C.R. Abernathy, J.D. MacKenzie, J.C. Zolper and E.S. Lambers, MRS Spring Meeting, SF, April 1996.
- "Er-doping of GaN and related alloys," S.J. Pearton, C.R. Abernathy, J.D. Mackenzie, R.N. Schwartz, R.G. Wilson, J.M. Zavada and R.J. Shul, MRS Spring 1996 Meeting, SF, April 1996-INVITED.
- "W, WSi_X and Ti/Al low resistance ohmic contacts to InGaN, InN and InAlN," C.B. Vartuli, S.J. Pearton, C.R. Abernathy, R.J. Shul, M. Lovejoy and H. Crawford, MRS Spring Meeting, SF, April 1996.
- "p-and n-type doping of GaN with Ca and O, J.C. Zolper, R.G.Wilson, S.J. Pearton and R.A. Stall MRS Spring Meeting, SF April 1996.
- "Temperature dependence of the electrical transport of carbon-doped GaN," W. Geerts, J.D. Mackenzie, C.R. Abernathy, S.J. Pearton and T. Schmiedel, MRS Spring Meeting, SF April 1996.
- "Ohmic Contacts to Wide Bandgap Semiconductors: HgSe and Au-Pt-ZnTe/ZnSe MQW's on p-ZnSe and Au on GaN", P.H. Holloway, J.F. Fijol, J. Trexler and S. Miller, TMS Annual Meeting, Anaheim, CA, Feb. 4-8, 1996, INVITED.
- "Dopant incorporation and non-equilibrium during low-temperature growth," I. Kuskovsky, G.F. Neumark, Presented at Spring, 1996 APS Meeting.
- "Time-resolved luminescence of heavily Nitrogen doped ZnSe," C. Kothandaraman, I. Kuskovsky, G.F. Neumark, and R.M. Park, Presented at Spring, 1996 APS Meeting.
- "IEEE/LEOS Distinguished Lecturer Award," P. Zory, Univ. of Ctrl. Fla., Mar. 18, 1996.

- "IEEE/LEOS Distinguished Lecturer Award," P. Zory, City Univ., London, England, UK Mar. 25, 1996.
- "IEEE/LEOS Distinguished Lecturer Award," P. Zory, Univ. Manchester, Manchester, England, UK, Mar. 27, 1996.
- "IEEE/LEOS Distinguished Lecturer Award," P. Zory, Univ. of Wales, Cardiff, Wales, UK, Apr. 1, 1996.
- "IEEE/LEOS Distinguished Lecturer Award," P. Zory, Univ. of New Mexico, Albuquerque, NM, Apr. 15, 1996.
- "IEEE/LEOS Distinguished Lecturer Award," P. Zory, Los Alamos National Laboratory, Los Alamos, NM, Apr. 19, 1996.
- "IEEE/LEOS Distinguished Lecturer Award," P. Zory, Univ. of Texas, Arlington, TX, Apr. 22, 1996.
- "IEEE/LEOS Distinguished Lecturer Award," P. Zory, Southern Methodist Univ. , Dallas, TX, Apr. 23, 1996.
- "IEEE/LEOS Distinguished Lecturer Award," P. Zory, Univ. of Wisconsin, Madison, WI, May 6, 1996.

Senior Research Thesis:

- "Growth by MBE and optical characterization of zincblende GaN, " Eric Michel, BS with Highest Honors,

Post Doctoral Associates:

Olga Kryliouk with Dr. Anderson

Graduate Students Supported:

Bruce Liu with Dr. Park
George Kim with Dr. Park
Lynn Calhoun with Dr. Park
in Hong with Dr. Pearton
K.N. Lee with Dr. Abernathy
Todd Dann with Dr. Anderson
Igor Kuskovsky with Dr. Neumark
Jeff Hsu with Dr. Zory
Jason O with Dr. Zory